Program Burn Algorithms Based on Detonation Shock Dynamics

Discrete Approximations of Detonation Flows with Discontinuous Front Models

J. B. Bdzil, D. S. Stewart [1] and T. L. Jackson

DX-division, Los Alamos National Laboratory, Theoretical and Applied Mechanics, University of Illinois and Center for Simulation of Advanced Rockets, University of Illinois

E-mail: dss@uiuc.edu; jbb@lanl.gov

In the design of explosive systems the generic problem that one must consider is the propagation of a well-developed detonation wave sweeping through an explosive charge with a complex shape. At a given instant of time the lead detonation shock is a surface that occupies a region of the explosive and has a dimension that is characteristic of the explosive device, typically on the scale of meters. The detonation shock is powered by a detonation reaction zone, sitting immediately behind the shock, which is on the scale of 1 millimeter or less. Thus, the ratio of the reaction zone thickness to the device dimension is of the order of 1/1000 or less. This scale disparity can lead to great difficulties in computing three-dimensional detonation dynamics. An attack on the dilemma for the computation of detonation systems has lead to the invention of sub-scale models for a propagating detonation front that we refer to herein as program burn models. The program burn model seeks not to resolve the fine scale of the reaction zone in the sense of a DNS simulation, instead the goal is to resolve the hydrodynamics in the inert product gases on a grid much coarser than required to resolve a physical reaction zone. We first show that traditional program burn algorithms for detonation hydrocodes used for explosive design are inconsistent and yield incorrect shock dynamic behavior. To overcome these inconsistencies, we discuss a new class of program burn models based on detonation shock dynamic (DSD) theory. This new class yields a more consistent and robust algorithm which better reflects the correct shock dynamic behavior.

[1]D. S. Stewart, Corresponding Author

1. INTRODUCTION

In the design of explosive systems the generic problem that one must consider is the propagation of a well-developed detonation wave sweeping through an explosive charge with a complex shape. At a given instant of time the lead detonation shock is a surface that occupies a region of the explosive and has a dimension that is characteristic of the explosive device, typically on the scale of meters. The detonation shock is powered by a detonation reaction zone, sitting immediately behind the shock, which is on the scale of 1 millimeter or less. Thus, the ratio of the reaction zone thickness to the device dimension is of the order of 1/1000 or less. This scale disparity can lead to great difficulties in computing three-dimensional (3D) detonation dynamics.

Assume (as we do for the rest of the paper) that the physical problem of modeling the dynamic propagation of the detonation and the motion of the reacted products in the following flow is completely described by a solution to the compressible Euler equations for a reactive flow, with a specified equation of state for the explosive and reaction rate of the form

$$e = e(p, v, \lambda), \qquad r = r(p, v, \lambda)\,,$$

where p, v, λ are the pressure, specific volume and the progress variable of chemical reaction. Note that $\lambda = 0$ corresponds to unreacted explosive and $\lambda = 1$ corresponds to completely reacted explosive. The prediction of the detonation dynamics can be achieved in principle by a direct numerical solution (DNS) of the Euler equations. In order to get a high quality solution to the reactive Euler equations, it is essential to have enough points in the reaction zone. Unfortunately even with modern algorithms, as many as 20-50 cells in the streamwise direction may be required to resolve the detonation reaction zone to sufficient accuracy so as to compute the detonation speed. When one then considers the consequences of such a fine scale for the reaction zone, combined with the requirement for global temporal and spatial accuracy in the meter-sized domain of the engineering device, huge computational resources are required [4] (even given todays TeraFlop parallel computing resources) for DNS of a detonation wave sweeping through a system.

The computational barrier to 3D design of explosive systems through direct simulation of the reactive Euler equations is not newly discovered, and dates back to the use of computers to design explosive systems that started systematically shortly after WWII. A dilemma of sorts presents itself. One needs to try to make predictions in engineering systems but one cannot overcome the stiff computational requirements needed to compute on the engineering device scale. One could compute DNS simulations that are resolved for very small dimensions, but those are at a minimum at least two orders of magnitude smaller than the engineering system scale. The dilemma posed above associated with trying to solve a physically correct but computationally intractable model is similar in spirit to direct simulation of turbulence on engineering device scales. In that discipline the need to resolve the physics of turbulence on larger engineering scales has led to the invention of classes of sub-scale models for turbulence and most recently to large eddy simulation.

An attack on the dilemma for the computation of detonation systems has lead to the invention of sub-scale models for a propagating detonation front that we refer to

herein as program burn (PB) models. The program burn model seeks *not* to resolve the fine scale of the reaction zone in the sense of a DNS simulation. The goal of a PB simulation (PBS) is to resolve the hydrodynamics in the inert product gases on a grid much coarser than that required to resolve a physical reaction zone. Thus a PBS must deposit a prescribed amount of energy (and more generally mass and momentum) into a *very few* number of computational cells behind a pre-calculated shock front. The effective reaction zone in a PBS is always the region behind a pre-calculated shock front where source terms are added to account for the deposition of energy. For practical reasons, the effective reaction zone is always constrained to be a finite number of cells thick (between one and four say).

The region where the source terms contribute, in the limit of zero cell thickness, limits to a sharp front across which there are jumps in the dependent state variables. The program burn source doses, while historically prescribed purely by the prescription of the discrete algorithm used in a particular code, must limit to a delta function source centered at the location of the sharp front, which is then externally prescribed by pre-calculating the shock location. The delta function source terms must, of course, be represented in the partial differential equations that represent the program burn model, independent of its discretization and the algorithms used to solve it. One thing is clear from this discussion, the solutions of the reactive Euler equations *are not* solutions of the equations of the program burn model.

In this paper we consider the following problem: How does one make consistent and robust discrete approximations of physical detonation flows with a finite length reaction zone as modeled by the reactive Euler equations, with a discrete approximation to a program burn model for which the reaction zone and shock is collapsed entirely to a single discontinuous front?

The whole scheme where a Program Burn model have solutions that are in some sense close to those of the Euler equations for a reactive flow depends very much on the accuracy of the approximate theory in regards to the shock dynamics. This issue must be decided irrespective of numerics. In Section 2 we briefly present direct numerical simulations (DNS) of the reactive Euler equations that are to be used as the benchmark calculations for the rest of the paper. The geometry considered will be either planar, cylindrical or spherical. For cylindrical/spherical geometry, curvature of the lead shock is present. In Section 3 we compare the solutions obtained from DNS to the recent asymptotic theory of detonation shock dynamics (DSD), a key ingredient of the more modern implementations of program burn. In Section 4 we regress somewhat by presenting the traditional pressure-based program burn (TPB) model; such a description is essential for understanding the rest of the paper. In addition, some numerical calculations are presented showing the strengths and weaknesses of the model. Section 5 presents presents various models aimed at improving the weaknesses inherent in the TPB model which curvature is present. This new class of models will be refered to as the modified pressure-based program burn models (MPB). There does not exist any reference which describes MPB, and so is presented here for the first time. Solutions obtained from MPB are compared with solutions obtained from TPB and DNS. The essential difference between TPB and MPB is that TPB uses a Huygen's construction for the shock propagation rule (shock propagates with the Chapman-Jouguet speed), while if curvature is

present, MPB uses a propagation rule based on DSD. Finally, conclusions are given in Section 6.

2. DIRECT NUMERICAL SIMULATIONS

In this section we present the reactive Euler equations that will be used as benchmark calculations to be compared with the program burn models presented in subsequent sections. We therefore assume that the DNS calculations are "exact", and that any differences in solution structure will be due to the various approximations inherent in the program burn models themselves.

For the DNS calculations, the conservative formulation of the reactive Euler equations are given by

$$\vec{U}_t + \vec{F}_x = \vec{G} + \vec{q}r, \tag{1}$$

where

$$\vec{U} = [\rho, \rho u, E, \rho\lambda]^T, \tag{2}$$

$$\vec{F} = \left[\rho u, \rho u^2 + p, u(E+p), \rho u\lambda\right]^T, \tag{3}$$

$$\vec{G} = -\frac{j}{x}\ \left[\rho u, \rho u^2, u(E+p), \rho u\lambda\right]^T, \qquad \vec{q} = [0,0,0,1]^T, \tag{4}$$

where ρ is the density, p the pressure, u the velocity, E the total energy defined by

$$E = \rho\left(e + \frac{1}{2}u^2\right), \tag{5}$$

e the specific internal energy, and λ the mass fraction of the deficient component ($\lambda = 0$ for unreacted material, $\lambda = 1$ for completely reacted material). The geometric source terms from the flow divergence are represented explicitly by $\vec{G}$. The choice of j determines the geometry; $j = 0$ for planar, $j = 1$ for cylindrical, or $j = 2$ for spherical geometry. If one assumes a cylindrical/spherical shock, the shock total curvature κ is related to the radius x from the center of the coordinate system by $\kappa = j/x$.

To close the system, constitutive laws for the internal energy and the reaction rate must be given. For illustration purposes, we take the example of a condensed phase explosive considered in [4] and used as a test problem in [1] and [2]. The equation of state is taken to be that of an ideal gas

$$e = \frac{p}{\rho(\gamma - 1)}\ -\ Q\lambda, \tag{6}$$

where γ is the ratio of specific heats and Q is the heat of reaction for the detonation. The reaction rate is given by

$$r = 2.5147\mu s^{-1}(1-\lambda)^{1/2}. \tag{7}$$

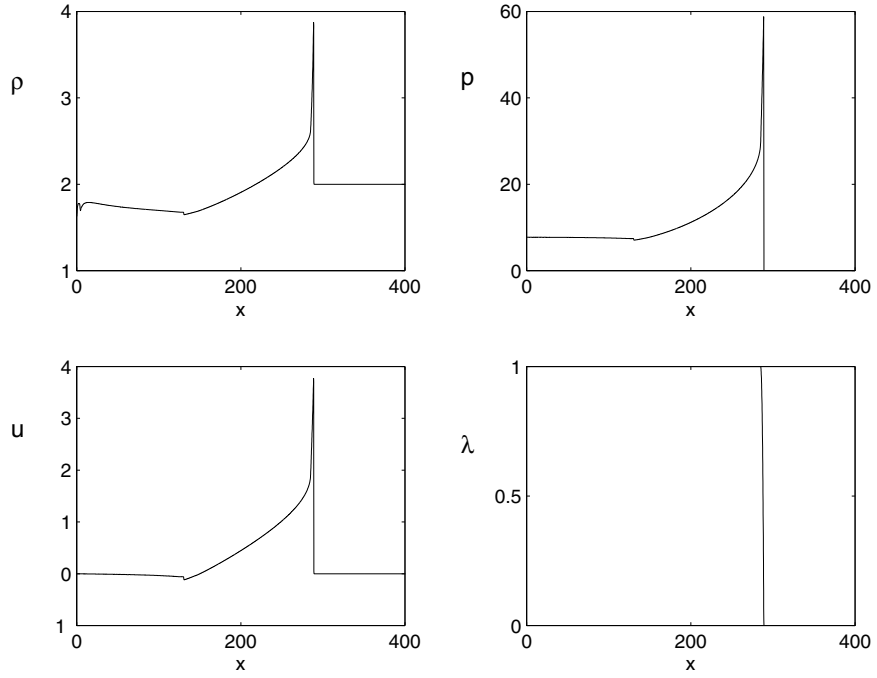

FIG. 1. Plot of the structure for the case $j = 1$ (cylindrical) at time $t = 40\mu s$.

The values $Q = 4mm^2/\mu s^2$ and $\gamma = 3$ are taken, with upstream conditions $p_o = 0$, $\rho_o = 2\ g/cc$ and $u_o = 0$. These values give a Chapman-Jouguet detonation speed of $D_{CJ} = 8mm/\mu s$, and a steady-state one-dimensional reaction zone length of $4mm$.

To carry out the DNS, these equations are solved by a high-resolution Euler solver, namely, a third-order TVD Runge-Kutta scheme with a fifth-order WENO spatial scheme, [6], [5] and [10]. The grid is assumed uniform with $\Delta x = 0.1mm$, which puts roughly 40 grid points in the reaction zone. Results for twice the number of grid points, and hence has 80 grid points in the reaction zone, gives essentially the same results. In all cases the CFL number was taken to be 0.4. Wave structures are presented in Figure 1. for the case of cylindrical geometry and in Figure 2 for the case of spherical geometry.

3. DSD ASYMPTOTIC THEORY AND COMPARISON TO DNS

In this section we briefly state the asymptotic theory of detonation shock dynamic (DSD) theory, a key ingredient of the program burn model that will be presented in subsequent sections. We also compare certain flow features between DSD theory and the DNS calculations of the reactive Euler equations presented in the previous section.

3.1. DSD Theory

Detonation shock dynamic (DSD) theory is an asymptotic theory which describes the motion of the detonation shock by means of a relation between the normal shock velocity D_n, the shock curvature κ, and their time derivatives. For a through review of the theory, its assumptions and limitations, see [7]. For our purposes here we shall

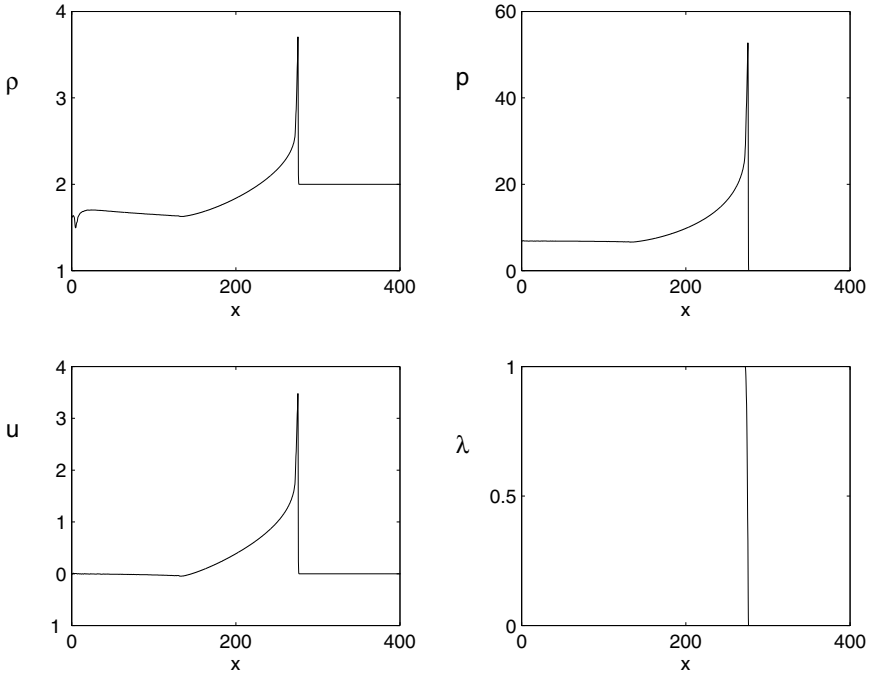

FIG. 2. Plot of the structure for the case $j = 2$ (spherical) at time $t = 40\mu s$.

only focus on the quasi-steady, one-dimensional theory. The relevant equations, consistent with the reactive Euler equations presented in a nearly integrable form that reflects the conserved first integrals of the governing equations if the flow were steady and plane, are

$$\frac{\partial(\rho U_n)}{\partial n} + \kappa\rho(U_n + D_n) = 0\,, \tag{8}$$

$$\frac{\partial(\rho U_n^2 + p)}{\partial n} + \kappa\rho U_n(U_n + D_n) \;= 0\,, \tag{9}$$

$$\frac{\partial}{\partial n}\left(e + pv + \frac{1}{2}U_n^2\right) = 0\,, \tag{10}$$

$$\frac{\partial\lambda}{\partial n} = -\frac{1}{U_n}\,(r)\;, \tag{11}$$

where n is the coordinate normal to the detonation front, and $U_n = u_n - D_n$ is the relative normal velocity in the shock-attached frame.

An alternative form of the energy equation, dubbed the *master equation*, is found by using the chain rule on $e(p, \rho, \lambda)$ in (10), using the mass equation to substitute for the spatial derivative of ρ, and then using the momentum equation to substitute for

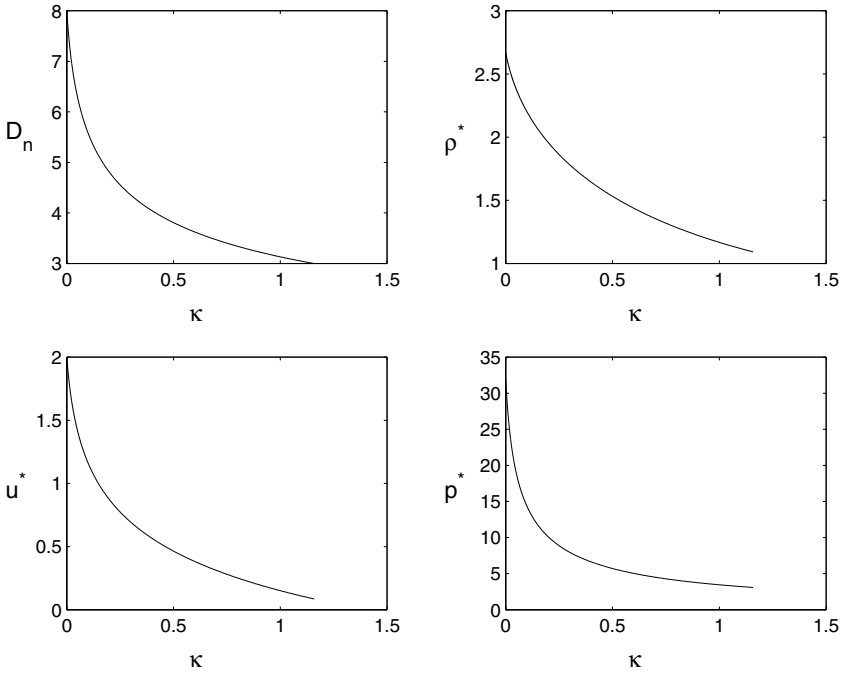

FIG. 3. Plot of the shock speed D_n and the star states as a function of κ.

the spatial derivative of the pressure p. With the standard definition of the sound speed by for an ideal EOS, $c^2 = \gamma p/\rho$, one obtains

$$(c^2 - U_n^2)\frac{\partial U_n}{\partial n} = Qr(\gamma - 1) - \kappa c^2(U_n + D_n)\,. \tag{12}$$

The *generalized CJ conditions* follow from the master equation. When the flow is locally sonic and the velocity gradient is finite it follows that when

$$\eta \equiv c^2 - U_n^2 = 0, \tag{13}$$

the right hand side of (12) must also be zero, i.e.,

$$\Phi \equiv Qr(\gamma - 1) - \kappa c^2(U_n + D_n) = 0. \tag{14}$$

The first condition is the *sonic condition*, while the second is the *thermicity condition*. These conditions hold for detonations that travel near or at the CJ detonation velocity. The simultaneous requirement that the sonic and thermicity conditions be satisfied require that there is a relationship between κ and D_n. For such solutions one can find the sonic, or star (*), states. The solution of this nonlinear eigenvalue problem can be done numerically if desired and the star states can be found as a function of the local curvature κ. A plot of the star states is shown in Figure 3 for the condensed phase example of the previous section. Note that for $\kappa = 0$, the star states are the CJ states, and $D_n = D_{CJ}$.

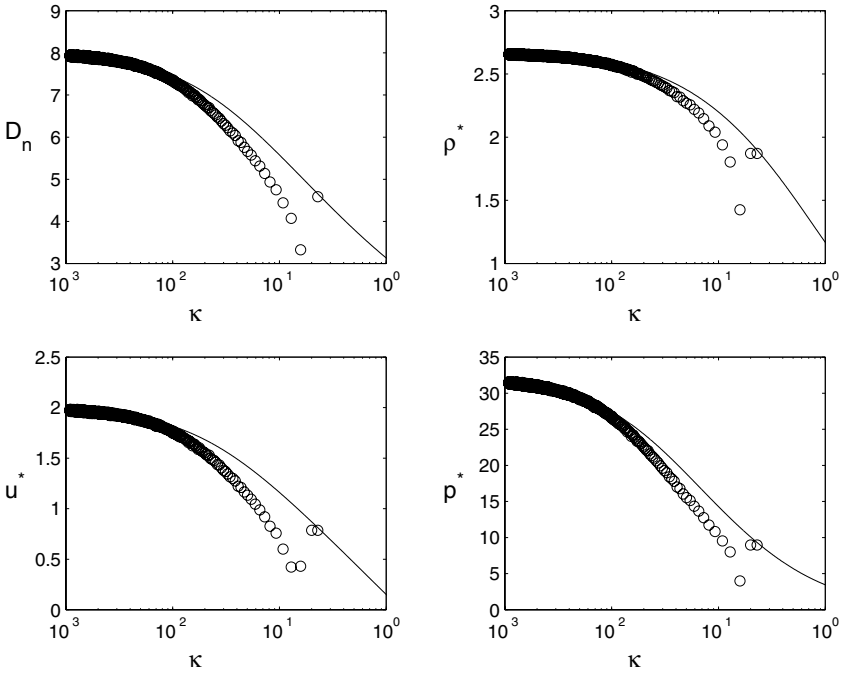

FIG. 4. Plot of D_n and the star states as a function of κ for DSD (solid) and DNS (circles). Cylindrical geometry.

3.2. DSD-DNS Comparisons

Comparisons of DSD theory with direct numerical simulations (DNS) have been carried out in [4] for the cases of detonation along a two-dimensional rate stick, in a converging channel, and a diverging channel. In all three cases the shock front locations as computed from DSD theory and from DNS were compared and good agreement between the two was found. Similar comparisons can be found in [2] and [3]. However, a simple and direct comparison between DSD and DNS can be carried out by considering cylindrical or spherical geometry where the curvature is explicitly known and the equations are essentially one-dimensional.

To compare with DSD theory, we show in Figures 4 and 5 the shock speed D_n and the star states as a function of curvature κ for cylindrical and spherical geometry, respectively. In each figure, the solid curve corresponds to DSD theory, and the circles correspond to the DNS calculations. The wave front was determined to be the value at which the reaction progress variable λ was 0.1; the speed is then the time derivative. Note the good agreement for both cylindrical and spherical geometries as the curvature goes to zero, i.e., the long time solution. For large values of the curvature, the agreement between the two diverge, either due to the transient effects of the DNS calculations at the earlier times or due to the first order and quasi-steady approximation of DSD theory where the time derivatives have been ignored.

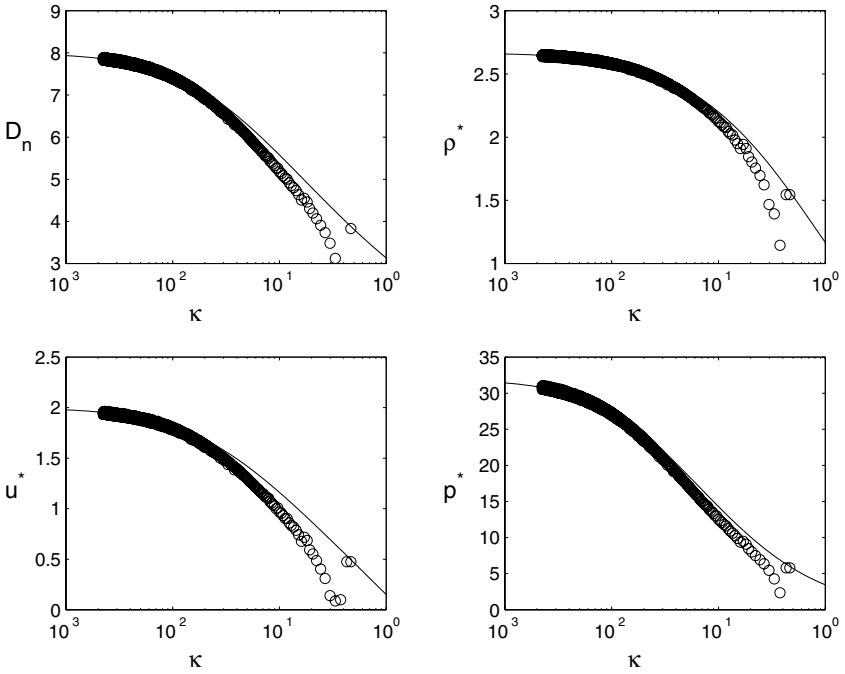

FIG. 5. Plot of D_n and the star states as a function of κ for DSD (solid) and DNS (circles). Spherical geometry.

4. TRADITIONALLY IMPLEMENTED PROGRAM BURN MODELS

In this section we discuss the basic ideas behind the implementation of program burn as it has traditionally been implemented in design hydrocodes used for explosive engineering. Although several versions exist, we shall discuss only one model, the traditional pressure-based program burn model (TPB). The other models have similar strengths and weaknesses, and only one model is sufficient to clarify the discussion.

Program burn was first posed as a numerical algorithm, not as a differential system. One of the earliest published references to an algorithm of this type is found in [9]. The algorithm has the following ingredients: i) There is a pre-determined, computational grid and a chosen algorithm for the inert hydrodynamics. The grid defines the domain of the explosive and the algorithms are used to solve the Euler equations for the (inert) explosive products. ii) A graded set of "burn-times", t_b, are assigned to each computational cell on the grid. The burn-times are the times that the detonation shock front crosses the coordinates of the initial position of the computational cell. The traditional way to compute the burn-times is to select the unreacted explosive geometry, pick the locus of an initial Chapman-Jouguet (CJ) detonation, and then compute the motion of the detonation shock emanating from the initial locus by means of a Huygen's construction. The Huygen's construction propagates the shock normal to itself at the constant CJ wave speed, D_{CJ}. iii) A cell-based algorithm either adds energy to designated burning cells or modifies the equation of state in cells during the interval of the shock passage over the cells, as dictated by the pre-calculated burn-times. The equation of state adjustment

has been done in various ways through either increments in the pressure or specific volume.

In what follows we give a description of a traditional pressure-based program burn algorithm which modifies the equation of state in the burning cells. The definitions of the burn-fraction, the burn-time field, pre-calculated shock motion and modification of the equation of state are key ingredients of the model.

4.0.1. Burn-fraction

Based on a previously calculated assignment, each cell is assigned a burn-time, t_b. If the present time of a computational cell is below the burn-time, $t < t_b$, then the cell is not burning and the burn-fraction Y is assigned zero. If $t > t_b$, then the burn-fraction must be calculated. The burn-fraction is usually assigned to be the volume fraction of the undisturbed cell that has been crossed by the detonation shock at that time, and hence has a computed value, $0 < Y < 1$. The details of the computation depends on the specific grid and algorithm and whether the burn-times are stored at cell centers or at the nodes. If the whole cell has been crossed the burn-fraction is simply $Y = 1$.

4.0.2. Burn-time field

Once the burn-fraction algorithm is selected, the discrete field of burn-fractions can be pre-calculated from the discrete field of burn-times. While (as the grid is resolved) the burn-times limit to a piecewise continuous field in the domain of the unshocked explosive, the discrete burn-fraction field must limit to a singular Heaviside function which is attached to the contours of the burn-time field (i.e., the pre-calculated shock position). The burn-time field is pre-calculated and the traditional way to do this is to use a Huygen's construction. Thus, once the unreacted explosive geometry is selected, the initial locus of an initial CJ detonation is picked, and the motion of the detonation shock that emanates from the initial locus is computed by means of a Huygen's construction.

4.0.3. Shock surface motion and the limits of discrete fields

The way to express these ideas mathematically is as follows. Let the burn-time field, which exists as a piecewise continuous field with a discrete representation on a grid which covers the domain of the unreacted explosive, be given by

$$t_b(\vec{x})\,.$$

Then, at a fixed time t_0, the shock locations are the contours of the burn-time field

$$\vec{x} = \vec{x}_s : t_0 = t_b(\vec{x_s})\,.$$

The limit of the discrete burn-fraction field at a time t_0 as the mesh is resolved is represented by the Heaviside function

$$H((\vec{x} - \vec{x}_s(t_0)) \cdot \hat{n})\,,$$

where $\hat{n}$ is the normal to the shock that points in the direction of propagation.

As an example, consider a one-dimensional detonation wave propagating with constant positive speed D_{CJ}. Then, according to Huygen's construction, we have

$$\frac{dx_s}{dt} = D_{CJ}, \tag{15}$$

where x_s is the location of the detonation front at time t. Integrating we get the motion rule for the front

$$x_s(t) = x_o + tD_{CJ}, \tag{16}$$

where x_o is the initial position. The domain $x < x_o$ is assumed to be completely reacted, and is unreacted for $x > x_o$. This relationship can be inverted to yield the burn-time field

$$t_b(x_s) = \frac{x_s - x_o}{D_{CJ}}. \tag{17}$$

For the discrete approximation, let the numerical grid have a uniform mesh, x_i, with grid spacing $\triangle x$. Then the discrete version of the burn-field can be written as

$$t_b(x_i) = \frac{x_i - x_o}{D_{CJ}}\ , \qquad \text{for} \quad x_i > x_o. \tag{18}$$

Note that the burn-time is not defined for $x_i \leq x_o$, which indicates that this region of the flow field has already reacted. Also note that the burn-time is piecewise continuous in the unreacted domain.

For the prescription of the burn-fraction, which we shall denote by Y_i, we update Y_i according to the rule

$$Y_i = \begin{cases} 0 & x_i > x_s, \\ \frac{x_s - x_i}{\triangle x} & x_s - \triangle x < x_i < x_s, \\ 1 & x_i < x_s - \triangle x. \end{cases} \tag{19}$$

This particular description of the burn-fraction is defined over a single cell. In the limit as $\triangle x \to 0$, we see that the burn-fraction approaches a Heaviside function. Figure 6 shows a sketch of the shock position as a function of time and a sketch of the burn-fraction Y. The use of the burn-fraction Y is described in more detail in the following section.

4.0.4. Modification of the equation of state and apparent weak detonation structure

In the traditional pressure-based program burn algorithm one assumes an equation of state for the inert products

$$e_{products}(p, v) \equiv e(p, v).$$

Since condensed explosives are being considered, the initial pressures (one barr) are extremely small compared to the detonation pressures behind the lead shock

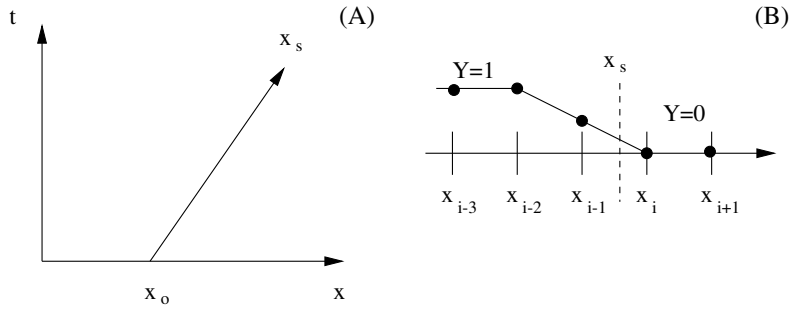

FIG. 6. (A) Sketch of the shock location $x_s(t)$ as a function of time. (B) Sketch of the burn-fraction Y on a discrete grid.

(hundreds of Kilo-bars) such that the pressure ahead of the shock in the unreacted explosive can be considered to be zero. This is similar to the strong shock approximation. In a PBS in the burning cells, where the burn-fraction Y is between zero and one, the equation of state is modified by replacing p with p/Y to obtain $e_{products}(p/Y, v)$. This is equivalent to replacing the pressure with a partial pressure which is reduced by the burn-fraction for that cell. When $Y = 1$, the equation of state for the products is recovered. Finally, in the unburnt cells in the unreacted explosive one must give an energy that is consistent with the heat of detonation. This is done in the following way. One considers the standard Rankine-Hugoniot relations for a gasdynamic discontinuity for a steady Chapman-Jouguet discontinuity traveling at laboratory speed D_{CJ}. One then sets the energy datum e_0 in the unreacted explosive consistent with that algebra. The equation of state for TPB can thus be written as

$$e = e_0\{1 - H((\vec{x} - \vec{x}_s(t))) \cdot \hat{n}\} \; + \; H((\vec{x} - \vec{x}_s(t)) \cdot \hat{n})\, e_{products}(p/Y, v). \quad (20)$$

An example of selecting e_0 is presented in the following section.

If we consider the pressure variation across the shock during a PB, the pressure starts out from zero and is brought up to a high value near the CJ-pressure. Indeed, when the burn-fraction Y is zero then the pressure is necessarily assumed to be zero, in fact the scheme computes the pressure based on an assumed equation of state and therefore the underlying hydrodynamic algorithm increments the pressure in such a way that the internal energy is assumed to be *finite*. A simple conclusion is that the effective reaction zone structure of traditional program burn starts at the unreacted state at the ambient pressure, and *not* at the shock state. If the program burn algorithm can be interpreted in terms of an effective distributed rate law, then the corresponding detonation structure looks like a weak detonation, and not a strong detonation. Note that the physically-based argument against a weak detonation structure is absent in a PBS, since the pre-calculated shock motion provides the sequenced burn-times for the cells that trigger the change in the equation of state in the vicinity of the shock. An alternative interpretation is that the PB scheme is a capturing scheme which intends to capture states that are near or at the steady state equilibrium CJ-values and hence cut off, or do not represent in any way, a physical reaction zone structure from the inert unreacted shock state (the von Neumann spike) to the sonic point that normally would be computed as part of the reaction zone in a DNS.

4.1. Example: Ideal EOS

To illustrate the traditional implementation of program burn, we will start with an equation of state (EOS) for the detonation products, $e(p, v)$ and be even more specific by using the gamma law equation of state

$$e(p, v) = \frac{1}{\gamma - 1}\frac{p}{\rho}.$$

4.1.1. CJ states

To compute the CJ-states, we first assume that the unburnt upstream state (with the strong shock approximation) ahead of the wave is given by

$$\rho = \rho_o, \quad u = 0, \quad p = 0, \quad e = e_o, \tag{21}$$

with e_0 unspecified at this point but will be chosen in the course of the analysis. Let $[\ ] = (\ )_o - (\ )_b$ denote the jump in a quantity across the interface from the o-state ($Y = 0$) to the completely burnt state ($Y = 1$) denoted by a b-subscript. The normal jump conditions across the interface moving with speed D_n are given by

$$[\rho(u_n - D_n)] = 0, \tag{22}$$

$$[\rho u_n(u_n - D_n) + p] = 0, \tag{23}$$

$$[E(u_n - D_n) + u_n p] = 0, \tag{24}$$

where E is the total energy defined earlier. With the assumption of the ideal EOS in the burnt products, the algebra of the above jump conditions are reduced to a quadratic equation in the normal particle velocity u_n, say. If we identify the speed D_n as the CJ value (D_{CJ}), the quadratic equation for u_n can be solved to give

$$u_n = \frac{D_{CJ} \pm \sqrt{D_{CJ}^2 - 2(\gamma^2 - 1)e_0}}{\gamma + 1}\,.$$

The CJ state is associated with the zero of the argument of the radical and lead to the identification of either the D_{CJ} in terms of the energy e_0 or vice a versa. Since we generally regard D_{CJ} as being given experimentally, we choose to write the condition as

$$e_0 = \frac{D_{CJ}^2}{2(\gamma^2 - 1)}. \tag{25}$$

Then the CJ states are

$$\rho_{CJ} = \rho_o\left(\frac{\gamma + 1}{\gamma}\right), \quad p_{CJ} = \frac{\rho_o D_{CJ}^2}{\gamma + 1}, \quad u_{CJ} = \frac{D_{CJ}}{\gamma + 1}\,. \tag{26}$$

It also follows simply that the CJ state is locally sonic. Note that in working out the Rankine-Hugoniot jump conditions across a program burn discontinuity, from the unreacted explosive to the burnt explosive where the burn-fraction Y is set equal to one, one obtains exactly the same Rankine-Hugoniot algebra as the reactive Euler equation where λ is set equal to one. Thus, the variation of a burn-fraction variable has no effect on the calculation of the CJ-states themselves.

As an example, we take the condensed phase explosive found in [4]. With $\gamma = 3$, $\rho_o = 2$ and $D_{CJ} = 8$, we get for the CJ states

$$\rho_{CJ} = \frac{8}{3}, \quad p_{CJ} = 32, \quad u_{CJ} = 2. \tag{27}$$

4.1.2. Equation of state with modified pressure and effects on the structure

In keeping with the notion that one replaces p with p/Y in the burning cells with $0 < Y \leq 1$, the ideal EOS becomes

$$e = \frac{1}{\gamma - 1}\frac{p}{Y\rho}.$$

Again one assumes that in the fresh material one has the same initial specific internal energy e_0, and the role of e_0 is the same as the heat of detonation.

To further analyze this structure let $U_n = u_n - D_n$ be the relative normal velocity in the shock-attached frame. For a quasi-steady traveling wave, the RH-relations hold throughout the structure, except now the internal energy has the dependence on the burn-fraction Y. As before, one can again solve the RH-relations

$$\rho U_n = -\rho_0 D_n$$

$$\rho U_n^2 + p = \rho_0 D_n^2$$

$$e + \frac{1}{2}U_n^2 + \frac{p}{\rho} = e_0 + \frac{1}{2}D_n^2, \quad \text{with} \quad e = \frac{p}{\rho Y(\gamma - 1)}\,,$$

for a quadratic equation in U_n with solutions

$$U_n = -\frac{[1 + (\gamma - 1)Y]D_n \pm \sqrt{D_n^2 - 2(\gamma - 1)Y[2 + (\gamma - 1)Y]e_0}}{2 + (\gamma - 1)Y}\,. \tag{28}$$

When $Y = 0$ the plus root corresponds to the unreacted flow state, and hence to the starting point for a weak detonation structure,

$$U_n = -D_n, \quad \text{or} \quad u_n = 0\,.$$

The root associated with the minus sign is pathological and has $U_n = 0$ or $u_n = D_n$, and corresponds to a finite pressure but infinite density. In contrast, the standard strong shock state $U_n = -(\gamma - 1)/(\gamma + 1)D_n$ is achieved if the equation of state $e = pv/(\gamma - 1)$ is used instead of the modified equation of state $e = (p/Y)v/(\gamma - 1)$.

The issue is which state is selected, and we turn to the acoustic character of the distributed structure next. From the fundamental definition of the sound speed,

$$c^2 = \frac{p/\rho^2 - \partial e/\partial \rho}{\partial e/\partial p} \ ,$$

we have

$$c^2 = \frac{p}{\rho}[1 + (\gamma - 1)Y].$$

Next, if we use the energy equation $e + p/\rho + U_n^2/2 = D_n^2/2 + e_0$ and use the definitions of e and the last result for c^2, we can eliminate p/ρ in favor of c and write an expression for the sonic parameter, η, as follows

$$\eta \equiv c^2 - U_n^2 = \left[e_0 + \frac{1}{2}(D_n^2 - U_n^2)\right](\gamma - 1)Y - U_n^2.$$

If the detonation wave starts out on the weak branch, then at $Y = 0$, $c = 0$, and $U_n = -D_n$, the sonic parameter $\eta = -D_n^2 < 0$, and the wave is supersonic at the point of the lead disturbance. In fact one can compute the sonic locus in a (U_n^2, Y) - plane by setting $c^2 = U_n^2$ to obtain

$$U_n^2 = \frac{\gamma^2(\gamma - 1)e_0 Y}{[1 + 1/2(\gamma - 1)Y]}. \tag{29}$$

The character of the structure of the (weak) detonation can be characterized by plotting its trajectory in a (U_n, Y) - plane. The weak CJ solution trajectory starts from the undisturbed state, $U_n = -D_n$ and terminates at the sonic state. Figure 7 shows this trajectory for the specific case of $D_n = D_{CJ}$. Note the square root behavior in U_n as $Y \to 1$, suggesting that the normal derivative has a square root singularity. This is due to the fact that the thermicity condition in the master equation does not vanish at the sonic point.

The other required ingredient for a weak detonation is a supersonic trigger. Ordinarily the supersonic trigger is regarded as aphysical. But for its application as a numerical algorithm, program burn assigns times at which the cell releases its energy. Specifically, the value of the burn-fraction is changed from $Y = 0$ to $Y = 1$ in proportion to how much of the particle cell has been crossed by an assumed shock wave. Therefore the distribution of times when the cell is crossed by a shock is know a-priori, and is used to create the supersonic trigger. For steady, one-dimensional flow for a CJ detonation, the burn-times simply and exactly reflect the CJ detonation velocity.

We note that the state variables do depend on the burn-fraction if the burn-fraction were distributed in a discrete representation; i.e., not resolved to a Heaviside step function. Then the burn-fraction distribution on a finite mesh has the appearance of a pseudo-reaction zone structure. In the following discussion, for convenience, we will model this distribution not by a difference based scheme, but instead modeled by an "effective" rate law in the steady detonation frame,

$$U_n \frac{\partial Y}{\partial n} = R(Y), \tag{30}$$

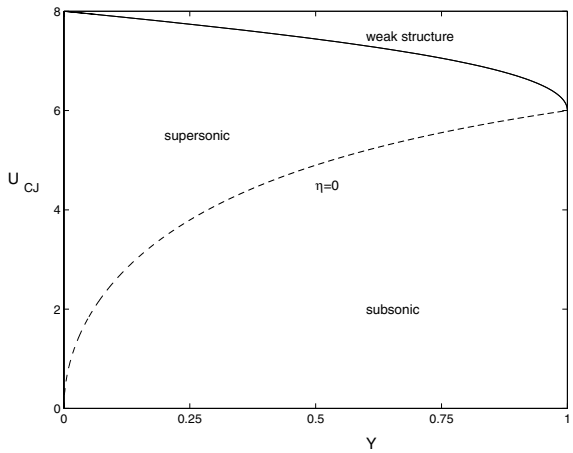

FIG. 7. U_{CJ}, Y-plane showing the trajectory of the weak, CJ detonation. The dash curve corresponds to the sonic locus given by (29) and the solid curve corresponds to the weak structure given by (28). (The strong structure branch is not shown.)

where $R(Y)$ is an effective rate. In actual practice this rate is not given at all, rather the numerical scheme that defines the burn-fraction merely makes an assignment for the increase in Y such that it goes to $Y = 1$ when the detonation shock crosses the computational cell completely and $R(Y)$ is inferred from the details of that assignment. But certainly $R(Y)$ is both grid and algorithm-dependent.

Integration of (30), with the weak-structure relation between U_n and Y and the condition that $Y = 0$ at $x = 0$ (which is equivalent to the specification of the triggering event at the program burn-time), leads to a distribution function $Y(x)$ which has the basic profile shown in Figure 6.

An important observation is that the thickness of the heat-release zone in the program burn reaction zone will be a function of the grid thickness and can be computed asymptotically as $O(\triangle x)$, such that as $\triangle x \to 0$, the program burn reaction zone vanishes, as measured relative to *any* physical length scale. Thus the effect of the numerical algorithm that $R(Y)$ imitates is to approximate a delta function, centered at the burn-times and spaces on the grid as dictated by the burn table.

4.2. Numerical results of TPB and comparisons to DNS

We present some numerical results comparing the solutions obtained using the traditional pressure-based program burn model (TPB) to the solutions obtained from a DNS calculation. We use the condensed phase explosive described in [4], [1], and [2]. The equations and numerical scheme for the DNS calculations were presented in detail in Section 2. For the TPB model we solve the corresponding non-reactive Euler equations with the EOS given by (20) and (25). Although current codes use a second-order scheme, we choose to use the same high-order scheme that is used for the DNS calculations to minimize errors resulting from different numerical algorithms, thus isolating any differences between the two solutions as rising from the various assumptions in the TPB model itself. To restate, we assume that the DNS calculations are "exact", and that any differences in solution structure will be due to the various approximations inherent in the TPB model. A mesh which

has only one grid point in the reaction zone ($\triangle x = 2mm$) is used. The reason we choose this particular grid size is that typical implementation of the program burn methodology uses only a fine enough grid to resolve the hydrodynamics behind the wave front. The grid chosen here is thus typical of that used in engineering practice; no attempt is made here to optimize nor study the effect of grid spacing on the solution structures.

Figure 7 shows the structure from the DNS (solid) and from the TPB (circles) calculations for planar geometry. In each case, the solutions were stopped when the shock location reached $x_s(t) = 100mm$. The arrival times of the two calculations is seen to be approximately the same (for DNS, $t = 12.72\mu s$; for TPB, $t = 12.05\mu s$), the 5% relative difference being due to differences in the grid resolutions and to the modeling assumptions of the reaction zone by the TPB model. Note how well the program burn model captures the overall structure. The only differences are seen in the density plot, where the DNS calculates a weak density jump downstream of the lead shock while the TPB calculations (with the coarser grid) does not, and in the shock region where the DNS calculations show a strong detonation profile and the TPB calculations show a weak detonation profile. We also ran long-time solutions, until the shock was located at $x_s(t) = 900mm$ (Figure 9.). The arrival times of the two calculations have a relative difference of less than 1% (for DNS, $t = 112.77\mu s$; for TPB, $t = 111.97\mu s$). Again, note how well the program burn model captures the overall structure.

The major weakness of the TPB model, however, occurs when curvature is present. Figure 10 shows the structure from the DNS and from the TPB calculations for the case of cylindrical geometry. Since the TPB uses a Huygen's construction to propagate the shock, we see that the arrival time of the shock to the location $x_s = 100mm$ is much quicker ($t = 12.075\mu s$) than that of the DNS calculations ($t = 15.3\mu s$); this represents roughly a 21% error in the arrival times. This large difference is not due to grid resolution, but rather to the TPB modeling of the shock speed using a Huygen's construction. Since Huygen's construction over-estimates the speed of the shock when curvature is present, we also see noticeable differences in the solution structures downstream of the lead shock. As in the planar case, we also ran long-time solutions, until the shock was located at $x_s(t) = 900mm$ (Figure 11); a close up look at the structure is shown in Figure 12). The arrival times of the two calculations is seen to be converging (for DNS, $t = 117.6\mu s$; for TPB, $t = 112.0\mu s$). In terms of the structure, the program burn model does seem to capture rather well the overall structure at the longer times. A closer look at the time behavior can be examined by comparing the shock speed and the star states to those obtained from DSD theory (see Figure 13). Note that the shock speed over-predicts the shock speed obtained from DSD, and that the star states are only asymptotic to the star states obtained from DSD theory.

The above results illustrates the strength and weaknesses of using the traditional program burn model to capture the physics of real detonations. For the planar case, the shock is propagated at the correct CJ speed, and the structure is represented well with only $1/40^{th}$ the number of grid points. This represents significant computational savings. However, when curvature is present there are major differences in not only the shock location but also in the structure of the solution. These differences are due to the fact that Huygen's construction over estimates the

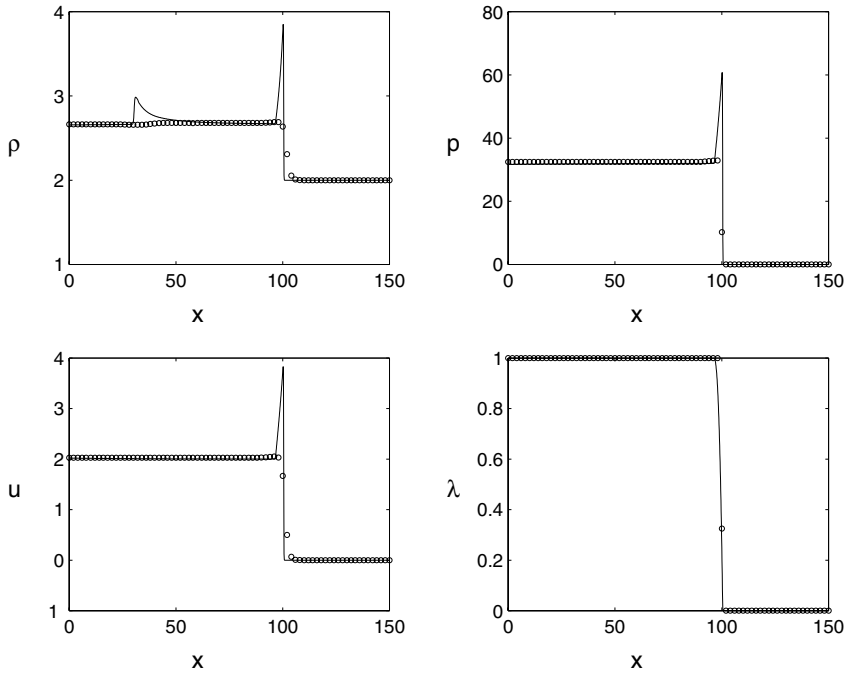

FIG. 8. Plot of the structure for planar geometry at $x_s(t) = 100mm$. Circles correspond to the TPB model ($t = 12.05\mu s$), and the solid curve to DNS ($t = 12.72\mu s$).

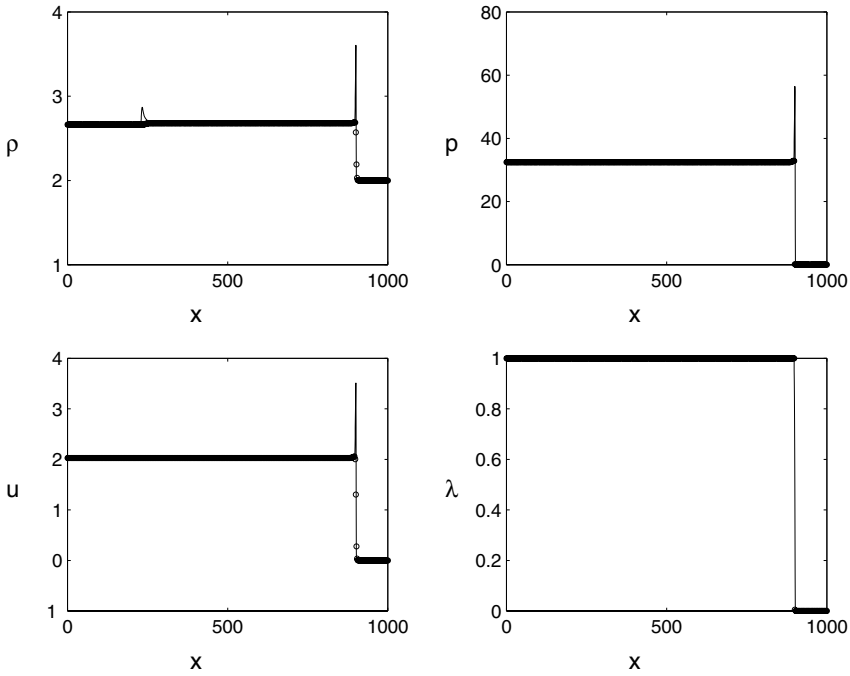

FIG. 9. Plot of the structure for planar geometry at $x_s(t) = 900mm$. Circles correspond to the TPB model ($t = 111.97\mu s$), and the solid curve to DNS ($t = 112.77\mu s$).

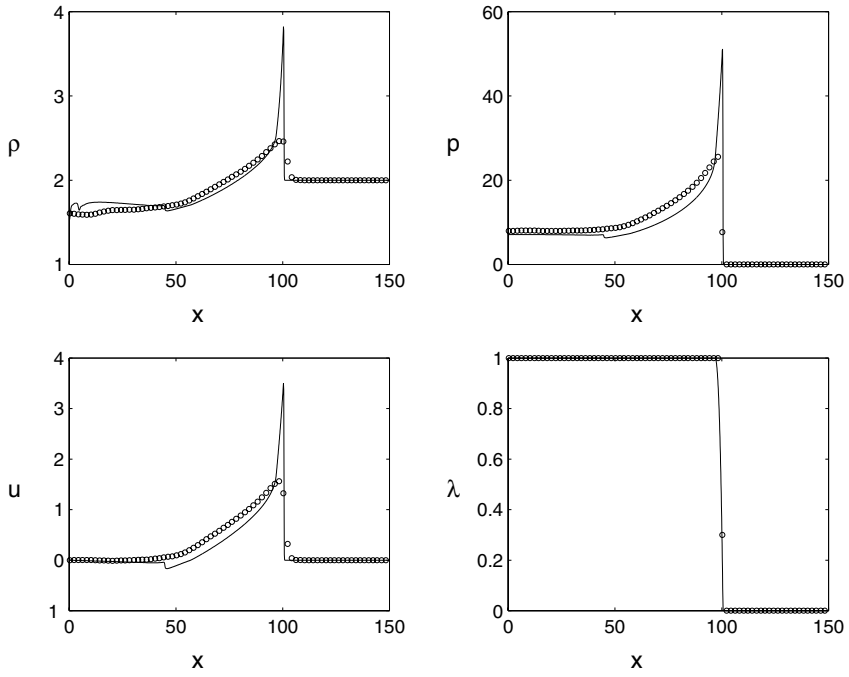

FIG. 10. Plot of the structure for cylindrical geometry at $x_s(t) = 100mm$. Circles correspond to the TPB model ($t = 12.075\mu s$), and the solid curve to DNS ($t = 15.3\mu s$).

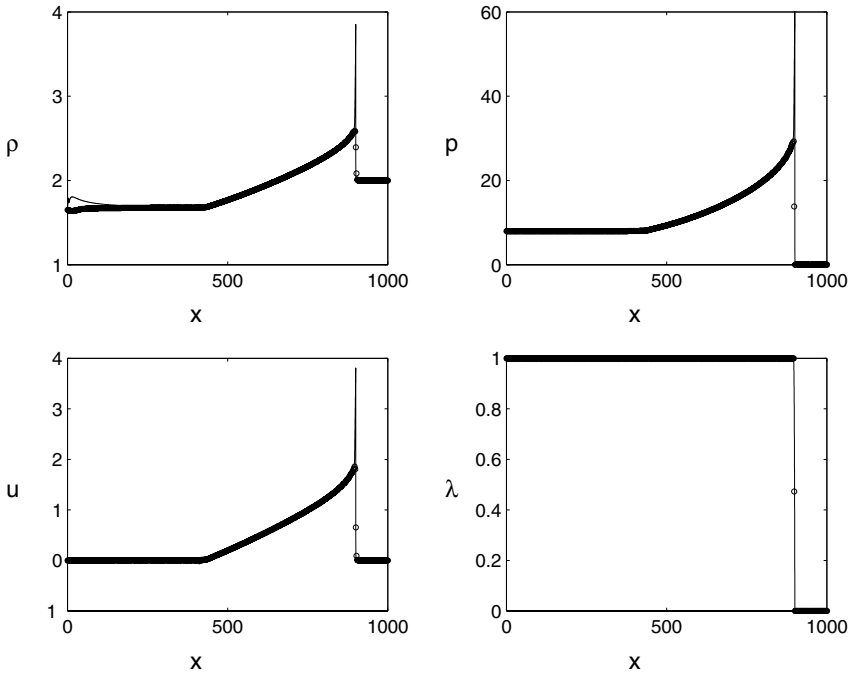

FIG. 11. Plot of the structure for cylindrical geometry at $x_s(t) = 900mm$. Circles correspond to the TPB model ($t = 112.0\mu s$), and the solid curve to DNS ($t = 117.6\mu s$).

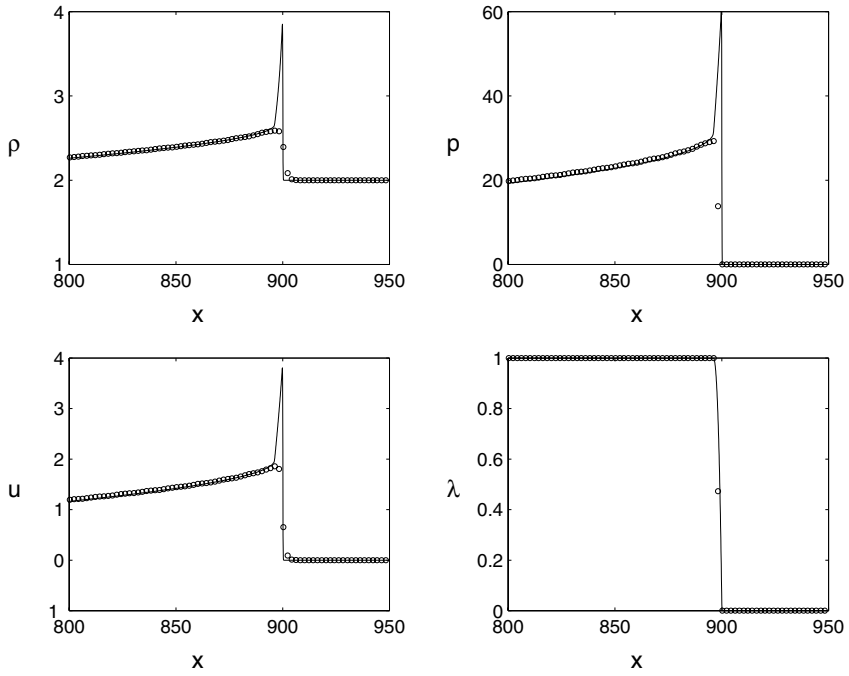

FIG. 12. Blow-up of the shock structure shown in Figure 12 for cylindrical geometry at $x_s(t) = 900mm$. Circles correspond to the TPB model ($t = 112.0\mu s$), and the solid curve to DNS ($t = 117.6\mu s$).

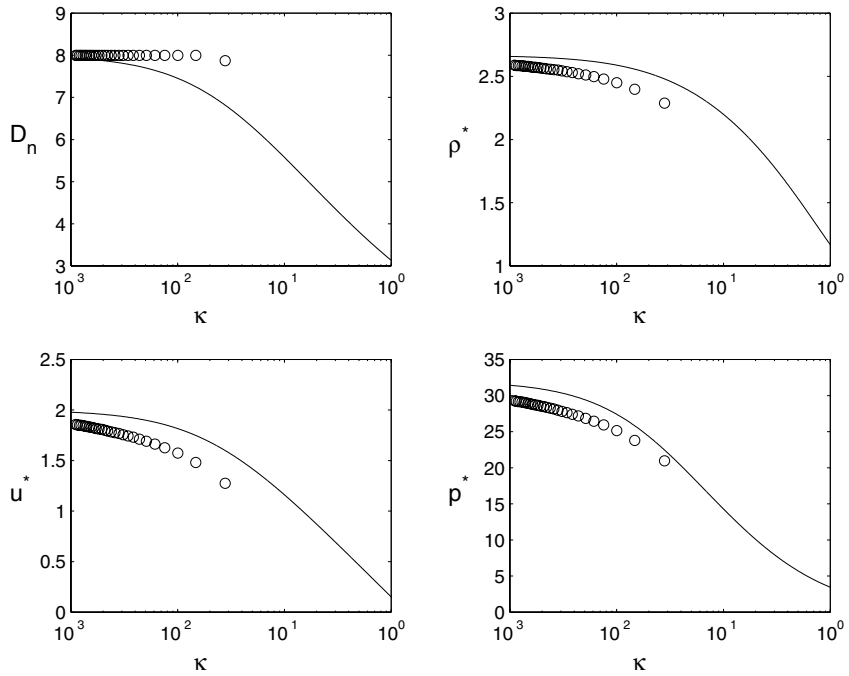

FIG. 13. Plot of D_n and the star states as a function of κ for DSD (solid) and TPB (circles).

speed of the propagating shock. Since curvature is present in almost all engineering devices, it is essential to properly take into account effects due to curvature. It is this weakness that we address in the subsequent section of this paper.

5. MODIFIED PRESSURE-BASED PROGRAM BURN MODELS (MPB)

In the previous section we have seen that when curvature is present, the traditional pressure-based program burn model is deficient in that the use of Huygen's construction over estimates the speed of the detonation front, leading to significant differences of the shock location and the structure between the DNS and the TPB simulations. A simple modification can be made by extending the theory to include a shock speed which is curvature dependent, as is found in DSD theory. In particular, we modify the burn-times to include the curvature dependence

$$\frac{dx_s}{dt} = D_n(\kappa), \tag{31}$$

and compute D_n according to DSD theory, given a particular equation of state. Once this modification has been made, the next natural question arises as to how best model the physical reaction zone? In the following subsections we present various models aimed at improving the TPB model when curvature is present.

5.1. Model I or MPB-1

In this model we modify the upstream internal energy to account for curvature affects, namely

$$e_0 = \frac{D_n^2}{2(\gamma^2 - 1)}, \tag{32}$$

where $D_n = D_n(\kappa)$ is the speed of the front with curvature dependence determined from DSD theory (see Section 3 for details). We refer to this modification of the burn-times and the upstream internal energy using DSD theory as the modified pressure-based program burn model I, or MPB-1.

Figure 14 shows results for the condensed phase explosive described in [4] in cylindrical geometry. Note that a simple change in the way the burn-times are computed and in the definition of the upstream internal energy can lead to significant changes in the errors. As before, the solutions were stopped when the shock location reached $x_s(t) = 100mm$. The arrival times of the two calculations is seen to be approximately the same (for DNS, $t = 15.3\mu s$; for MPB-1, $t = 14.2\mu s$), the 7% relative difference being a major improvement when compared to the 21% relative difference in the arrival times between TPB and DNS. Comparing Figures 10 and 14, we see that the MPB-1 captures the overall physics better than the TPB model. The long time solution, when $x_s(t) = 900mm$, is shown in Figures 15 and 16, and should be compared to Figures 11 and 12, respectively, from the TPB model.

However, the MPB-1 fails to capture the correct sonic (or star) states. Capturing the correct star states is an important indicator of how well a given scheme does since both the strong detonation and the weak detonation should terminate at this point. We plot in Figure 17 the star states as computed here from the numerical

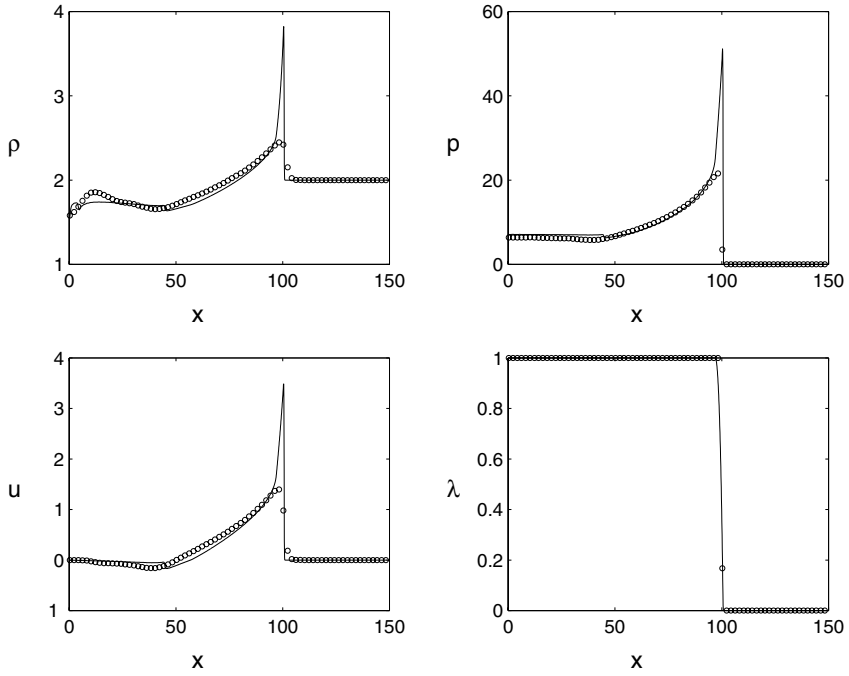

FIG. 14. Plot of the structure for cylindrical geometry with $\triangle x = 2mm$ at $x_s(t) = 100mm$. Circles correspond to the MPB-1 ($t = 14.2\mu s$), and the solid curve to DNS ($t = 15.3\mu s$).

simulations to the star states determined from DSD theory. There is still an unacceptably large discrepancy in the star states. This shows that although the correct speed can be modeled using DSD theory, the overall structure is still not correct. This is a major deficiency of the model. We show in Figure 18 the star states for a grid resolution of $\triangle x = 0.5mm$. In these calculations the energy released is still over a single grid point, so reducing $\triangle x$ reduces the effective reaction zone. Alternatively, one could keep the reaction zone fixed so that reducing $\triangle x$ would imply more points in the reaction zone; we have not done this comparison but plan to do so in the future. Note that there is better agreement in the star states. Also note that the oscillations in the shock speed D_n observed in Figure 17 have been reduced by grid resolution. A further refinement would violate the spirit of the program burn model, and so no further grid refinements were carried out.

One final comment. In the mid-1990's Bdzil and Stewart modified major TPB codes at Los Alamos National Laboratory to include curvature dependence using DSD theory (which we referred here as the MPB-1). The results of their work was not published at the time and to date, no other comparisons between TPB and MPB-1 to DNS have been published. To our knowledge this is the first discussion of these models.

Blow-up of the shock structure shown in Figure 15 for cylindrical geometry with $\triangle x = 2mm$ at $x_s(t) = 900mm$. Circles correspond to the MPB-1 ($t = 116.76\mu s$), and the solid curve to DNS ($t = 117.6\mu s$).

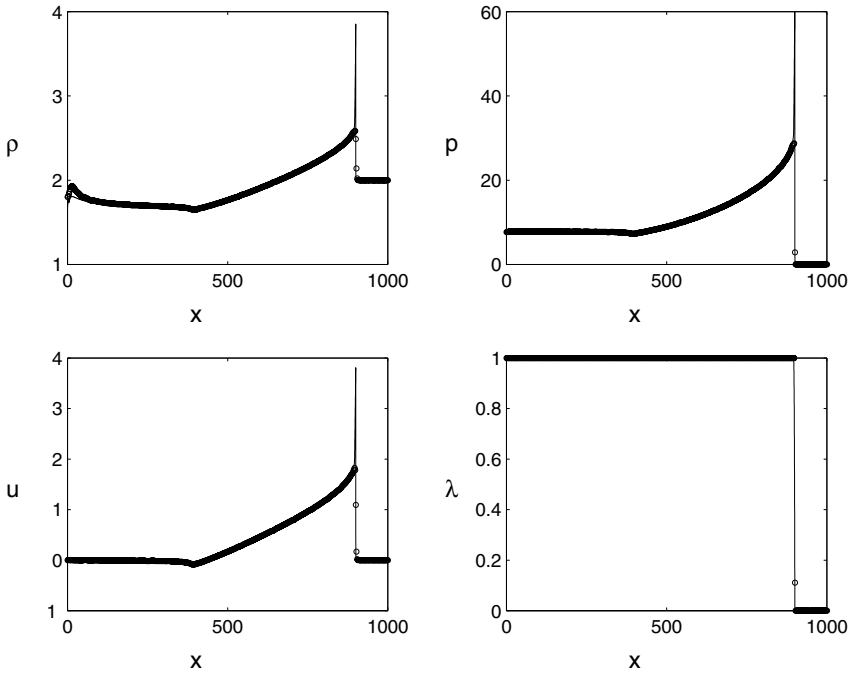

FIG. 15. Plot of the structure for cylindrical geometry with $\triangle x = 2mm$ at $x_s(t) = 900mm$. Circles correspond to the MPB-1 ($t = 116.76\mu s$), and the solid curve to DNS ($t = 117.6\mu s$).

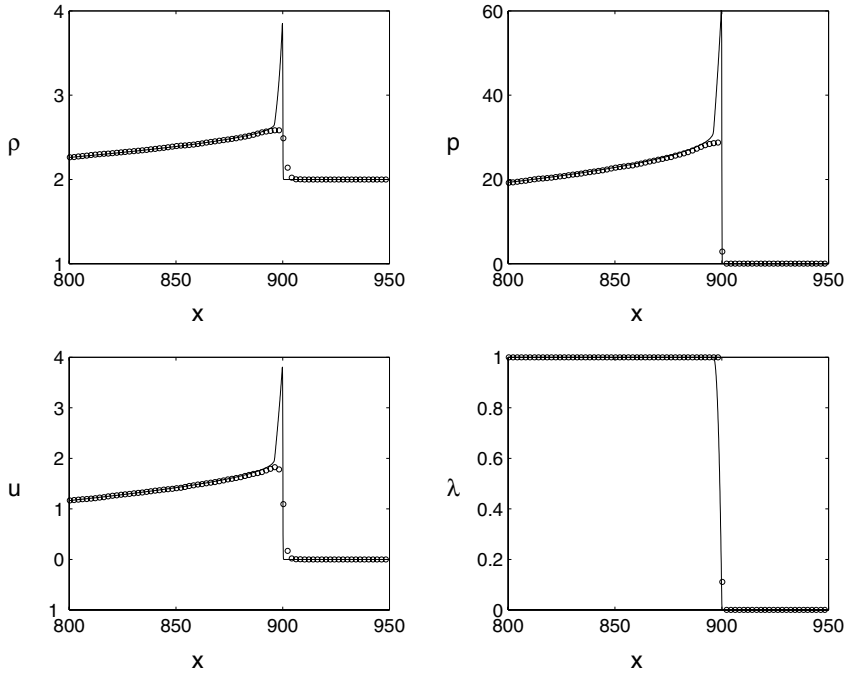

FIG. 16. Blow-up of the shock structure shown in Figure 15 for cylindrical geometry with $\triangle x = 2mm$ at $x_s(t) = 900mm$. Circles correspond to the MPB-1 ($t = 116.76\mu s$), and the solid curve to DNS ($t = 117.6\mu s$).

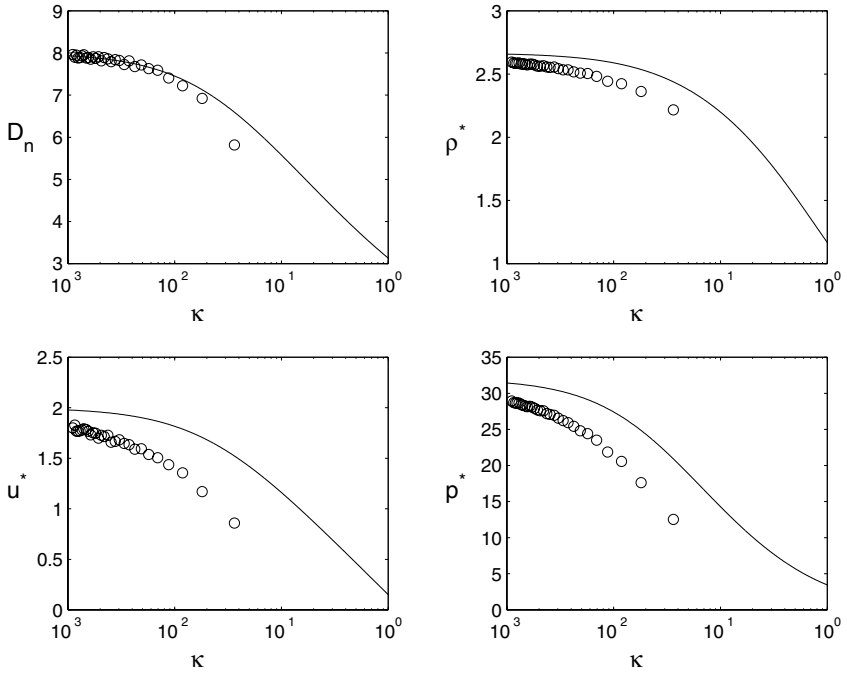

FIG. 17. Plot of D_n and the star states as a function of κ for DSD (solid) and MPB-1 (circles) with $\triangle x = 2mm$.

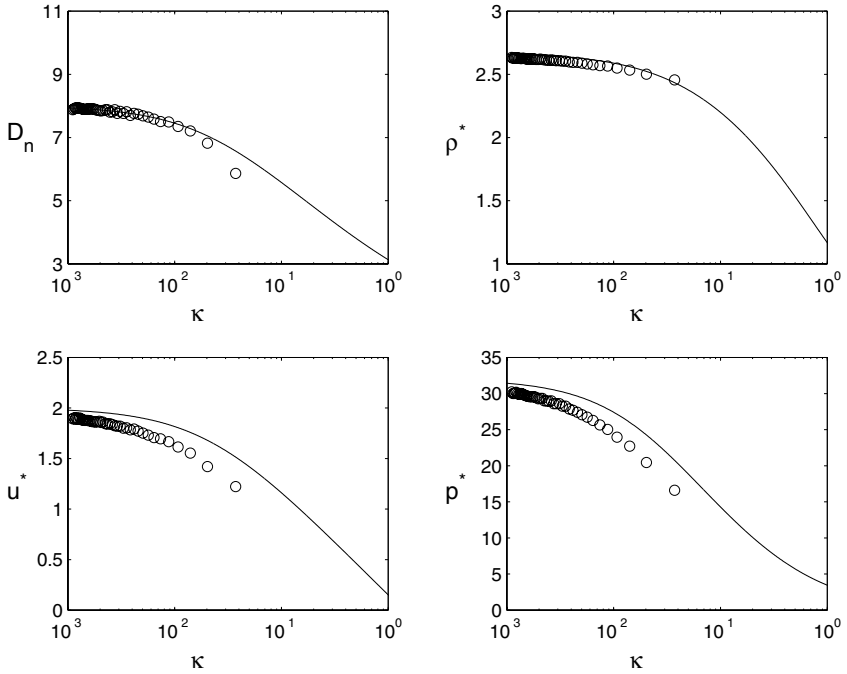

FIG. 18. Plot of D_n and the star states as a function of κ for DSD (solid) and MPB-1 (circles) with $\triangle x = 0.5mm$.

5.2. Model II or MPB-2

In this model we keep the specification of the upstream internal energy

$$e_0 = \frac{D_{CJ}^2}{2(\gamma^2 - 1)}, \tag{33}$$

but modify the length scale of the program burn reaction zone to mimic the reaction zone thickness of the physical problem. That is, in the TPB model, the program burn reaction zone thickness is kept at one grid cell, independent of grid resolution. Thus, as the grid size becomes smaller, so does the program burn reaction zone thickness. We modify this by pre-assigning a program burn reaction zone thickness which has a length scale of approximately the same size as the physical problem, such that as the grid size becomes smaller, the program burn reaction zone stays fixed and the number of computational cells within it increases. In particular, if L is the program burn reaction zone length, then we select a value of k, the number of computational cells within the zone, such that $k\triangle x = L$. For the condensed phase example, the physical reaction zone length is $4mm$ when no curvature is present, and slightly less when curvature is present. We fix $L = 4mm$ for simplicity. We refer to this modification of the burn-times using DSD theory and distributed program burn reaction zone thickness as the modified pressure-based program burn model II, or MPB-1I.

We show in Figures 19 and 20 results for two different grid resolutions. In the first figure the grid resolution is $2mm$ and so we chose $k = 2$, giving two gird points within the reaction zone. Note that the shock structure is quite different from that of Model I, MPB-1 (compare Figure 14). When the upstream value of e_0 depends on curvature, the structure looks like a weak detonation; when e_0 is fixed, the structure looks like a strong detonation. Decreasing the grid size to $0.5mm$, and hence increasing k to 8, not only captures the overall flow structure better than the coarse resolution, but also better captures the detonation structure. The same is true at the longer times, where we show a blow up of the structure for a grid resolution of $2mm$ with $k = 2$ (Figure 21) and a grid resolution of $0.5mm$ with $k = 8$ (Figure 22).

5.3. Model III or TPB-3

In this section we present another class of models aimed at improving the TPB models when curvature is present. The equations governing this new class of models are given by

$$\vec{U}_t + \vec{F}_x = \vec{G} + \vec{Q} R_{\delta(x - x_s(t))}, \tag{34}$$

where

$$\vec{U} = [\rho, \rho u, E]^T, \tag{35}$$

$$\vec{F} = \left[\rho u, \rho u^2 + p, u(E + p)\right]^T, \tag{36}$$

$$\vec{G} = -\frac{j}{x} \left[\rho u, \rho u^2, (E + p)u\right]^T, \qquad \vec{Q} = [Q_1, Q_2, Q_3]^T, \tag{37}$$

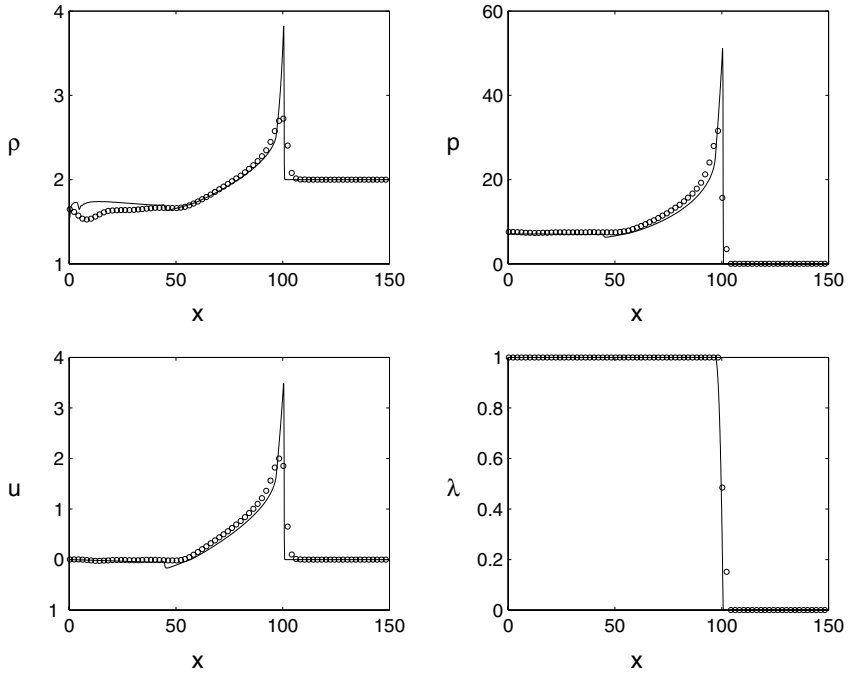

FIG. 19. Plot of the structure for cylindrical geometry with $\triangle x = 2mm$ at $x_s(t) = 100mm$, with $k = 2$. Circles correspond to the MPB-2 ($t = 14.5\mu s$), and the solid curve to DNS ($t = 15.3\mu s$).

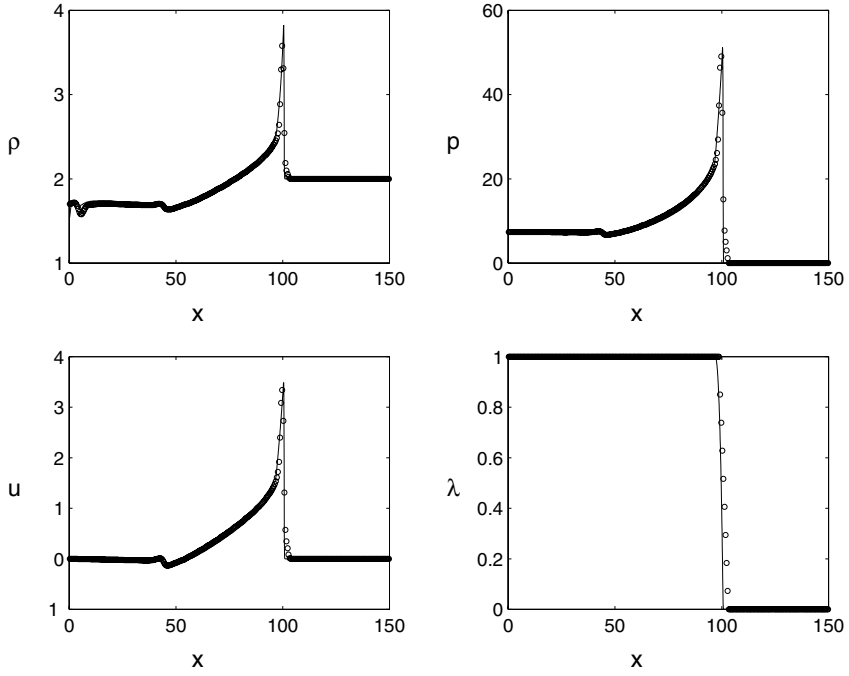

FIG. 20. Plot of the structure for cylindrical geometry with $\triangle x = 0.5mm$ at $x_s(t) = 100mm$, with $k = 8$. Circles correspond to the MPB-2 ($t = 14.5\mu s$), and the solid curve to DNS ($t = 15.3\mu s$).

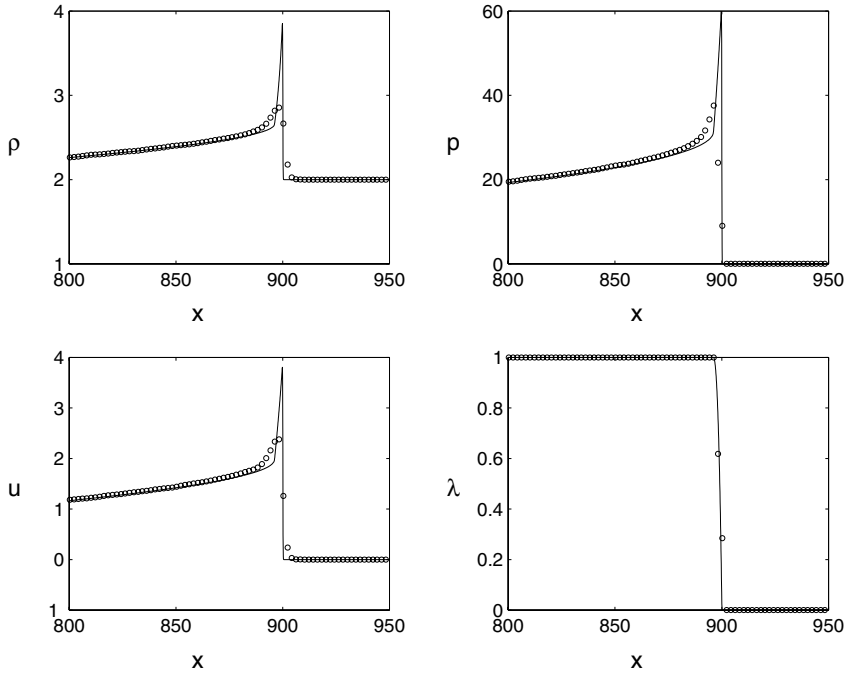

FIG. 21. Plot of the structure for cylindrical geometry with $\triangle x = 2mm$ at $x_s(t) = 900mm$, with $k = 2$. Circles correspond to the MPB-2 ($t = 14.5\mu s$), and the solid curve to DNS ($t = 117.6\mu s$).

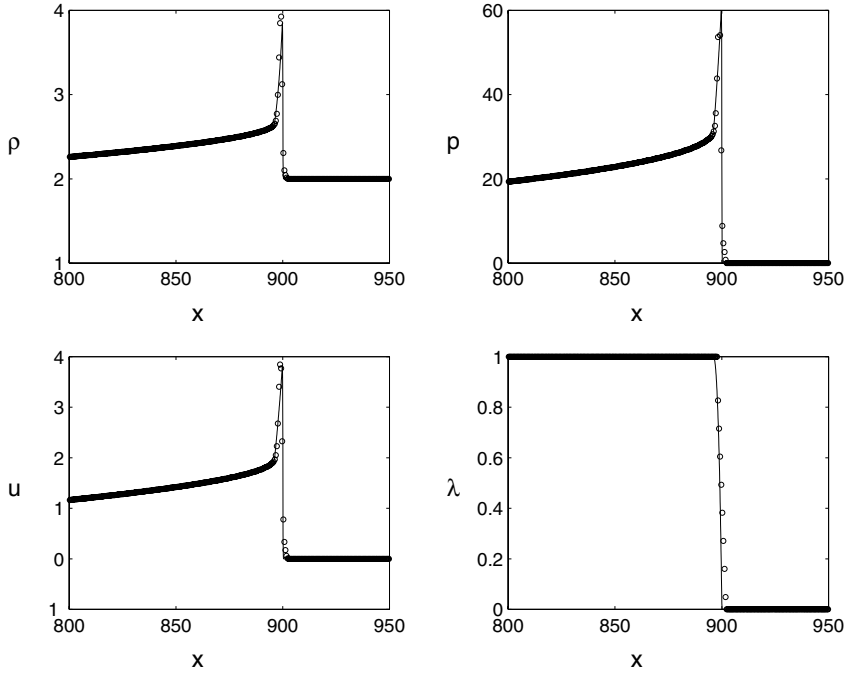

FIG. 22. Plot of the structure for cylindrical geometry with $\triangle x = 0.5mm$ at $x_s(t) = 900mm$, with $k = 8$. Circles correspond to the MPB-1I ($t = 14.5\mu s$), and the solid curve to DNS ($t = 117.6\mu s$).

and again E is the total energy defined by

$$E = \rho\left(e + \frac{1}{2}u^2\right), \tag{38}$$

and e is the internal energy. Specific choices for e will be given below. Note that $R_{\delta(x-x_s(t))}$ is a delta function centered on the program shock locus $x = x_s(t)$ and is assumed to be known. The geometric source term $\vec{G}$ is identical in its first three components to its DNS counterpart. The choice of $\vec{Q}$ and R_δ will be made later in the course of the analysis.

We will consider two models for the internal energy. The first model mimics the TPB model and is written, for an ideal gas, as

$$e = \frac{p/Y}{\rho(\gamma - 1)}, \tag{39}$$

where γ is the ratio of specific heats and Y is the burn fraction with $0 \le Y \le 1$. The upstream value of the internal energy is given by (32). We will refer to this as Model IIIa or TPB-3a. The second model is the standard equation of state without the burn fraction, and for an ideal gas is written as

$$e = \frac{p}{\rho(\gamma - 1)}. \tag{40}$$

The upstream value of the internal energy is given by $e_0 = 0$, consistent with the strong shock approximation. We will refer to this as Model IIIb oe TPB-3b. To completely specify the program burn PDEs one must identify the source term strength $\vec{Q}$. Various specifications are made and analyzed below.

One way to determine values of $\vec{Q}$ is to make the quasi-steady assumption and neglect the explicit dependence of curvature in the program burn equations. The lead shock is taken to be at $x = x_s(t)$ with speed D_n, which can depend on curvature and is given by the D_n, κ relation from DSD theory. Across the shock we allow for doses to the mass, momentum and energy, and the jump conditions across the program-burn shock are given by

$$[\rho(u_n - D_n)] = Q_1[Y], \tag{41}$$

$$[\rho u_n(u_n - D_n) + p] = Q_2[Y], \tag{42}$$

$$[E(u_n - D_n) + u_n p] = Q_3[Y], \tag{43}$$

where $[\phi] = \phi_o - \phi^*$, and the star states are determined using DSD theory. Note that in writing down these normal jump conditions we assumed that $R_\delta = dY/dn$, where n is the normal coordinate. Since the shock location is known, and both the upstream states and the star states are known, the jump relations become formulas for explicit evaluation of the doses $\vec{Q}$.

Evaluating the jumps leads to the following specifications for the components of $\vec{Q}$

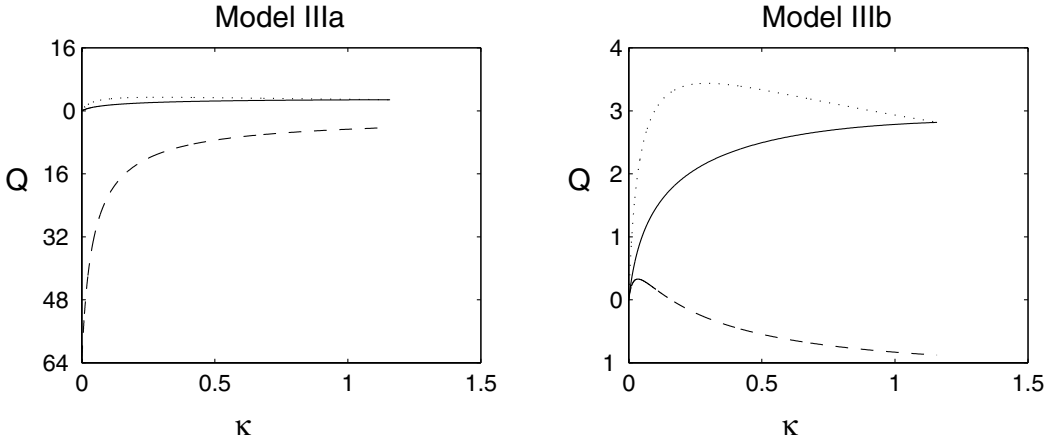

FIG. 23. Plot of Q_1 (solid), Q_2 (dotted) and Q_3 (dashed) as a function of κ for models TPB-3a and TPB-3b, respectively.

$$\begin{aligned} Q_1 &= \rho_o D + \rho^*(u^* - D_n), \\ Q_2 &= p^* + \rho^* u^*(u^* - D_n), \\ Q_3 &= \rho_o e_o D_n + E^*(u^* - D_n) + u^* p^* \ . \end{aligned} \tag{44}$$

A plot of the star states was given previously in Figure 3 for the condensed phase explosive example given in [4]. The values of $\vec{Q}$ as computed from these formulas is shown in Figure 23 for both TPB-3a and TPB-3b, respectively. Results for the two models are given in Figures 24 through 27 for TPB-3a and in Figures 28 through 31 for TPB-3b. These results are in qualatative agreements with TPB (Model I).

6. CONCLUSIONS

We have presented a comprehensive review of the traditional program burn algorithm, and have compared solutions to those of a direct numerical simulation. It was shown that if curvature is present, the traditional program burn alogrithm overpredicts the shock speed. A slight modification to the burn times, based on detonation shock dynamic theory, can correct the shock speed difficulty. Various models are presented and compared to DNS; overall, the results of Model II (constant upstream value for the internal energy, fixing the program burn reaction zone length) give results which surprisingly capture the DNS structure, even with a grid resolution of about 5 times larger than that of the DNS. We are currently investigating these models in two-dimensional geometries and extension to real product equations of state.

ACKNOWLEDGMENT

The work of D. S. Stewart was supported by a contract with the Department of Energy, DOE-LANL under the present contract I2933-0019 and previous contracts with LANL. T. L. Jacson was supported by a previous LANL contract and the DOE contract that supports the UIUC ASCI center, Center for Simulation of Advanced Rockets. J. B. Bdzil is supported at Los Alamos by the Department of Energy.

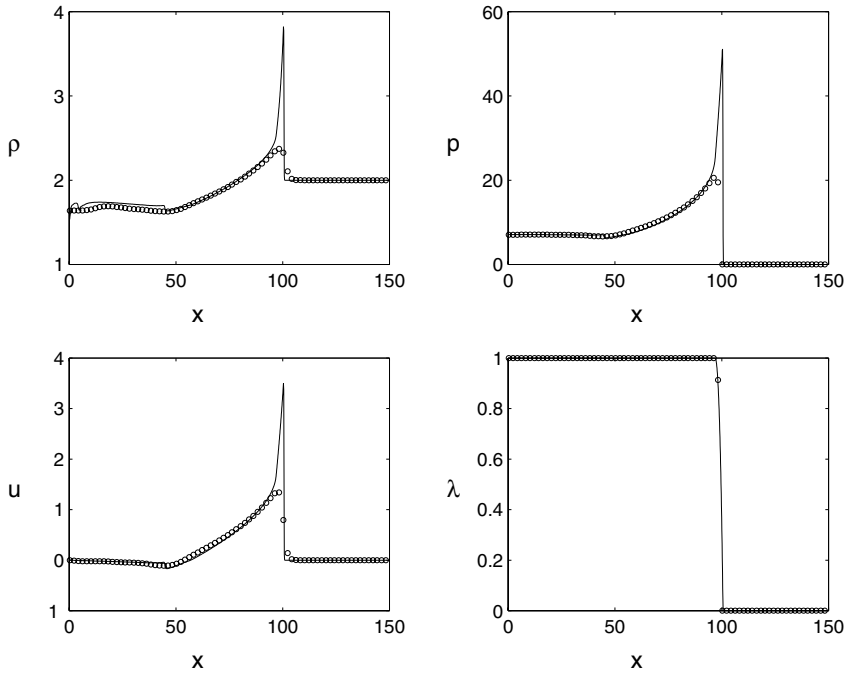

FIG. 24. Plot of the structure for cylindrical geometry with $\triangle x = 2mm$ at $x_s(t) = 100mm$. Circles correspond to the model TPB-3a ($t = 14.2\mu s$), and the solid curve to DNS ($t = 15.3\mu s$).

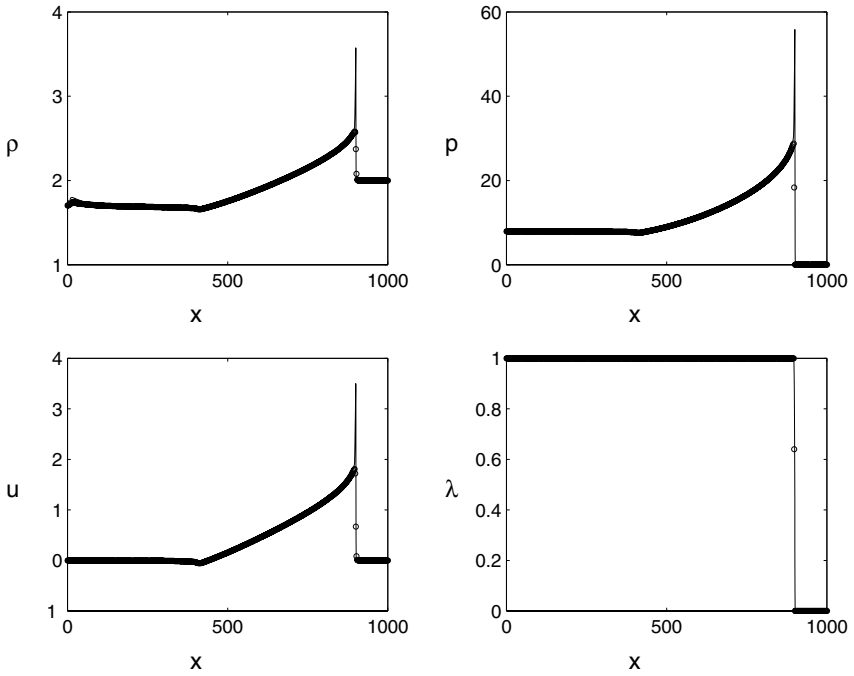

FIG. 25. Plot of the structure for cylindrical geometry with $\triangle x = 2mm$ at $x_s(t) = 900mm$. Circles correspond to the model TPB-3a ($t = 116.2\mu s$), and the solid curve to DNS ($t = 127.5\mu s$).

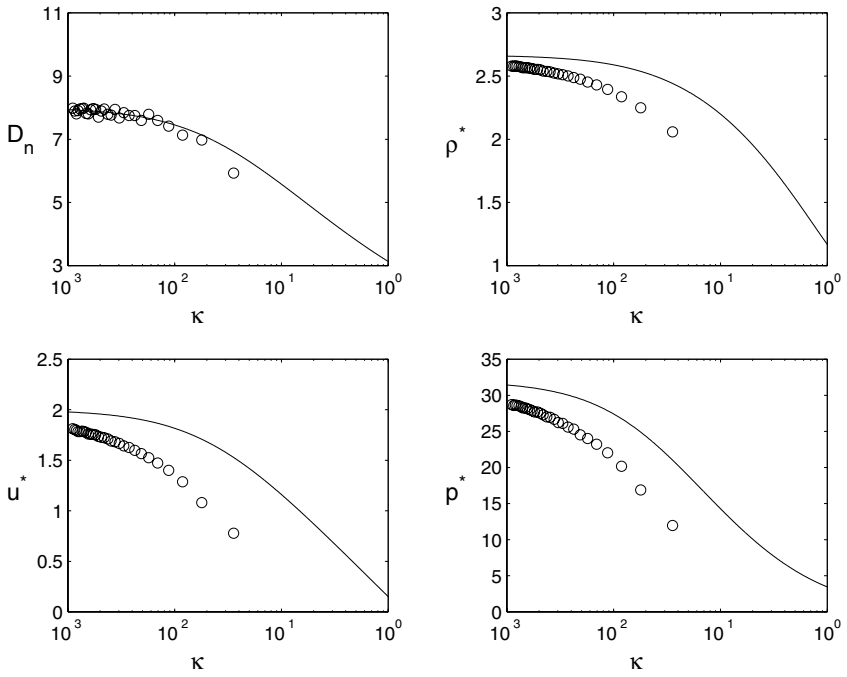

FIG. 26. Plot of D_n and the star states as a function of κ for DSD (solid) and model TPB-3a (circles) with $\triangle x = 2mm$.

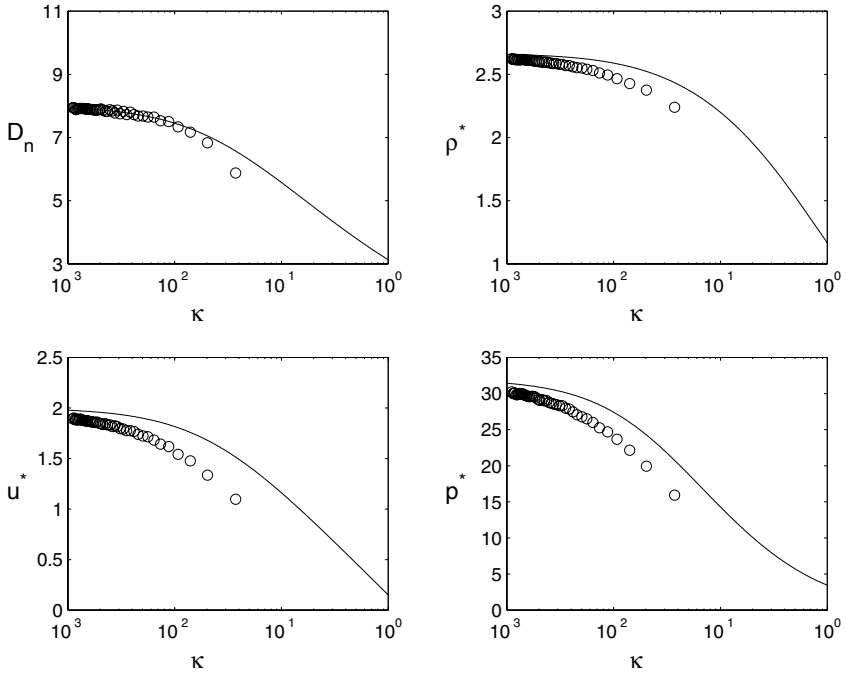

FIG. 27. Plot of D_n and the star states as a function of κ for DSD (solid) and model TPB-3a (circles) with $\triangle x = 0.5mm$.

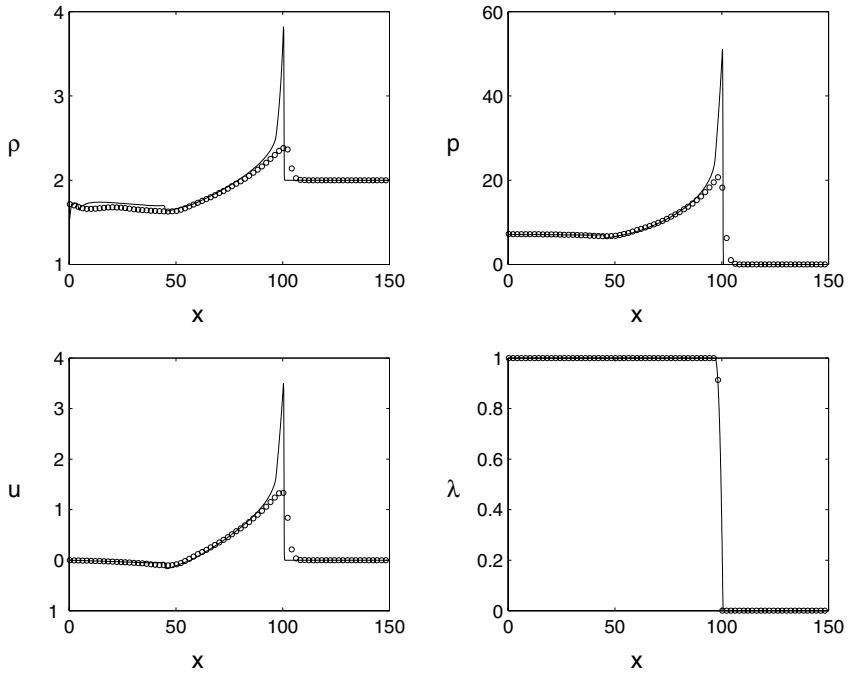

FIG. 28. Plot of the structure for cylindrical geometry with $\triangle x = 2mm$ at $x_s(t) = 100mm$. Circles correspond to the model TPB-3b ($t = 14.2\mu s$), and the solid curve to DNS ($t = 15.3\mu s$).

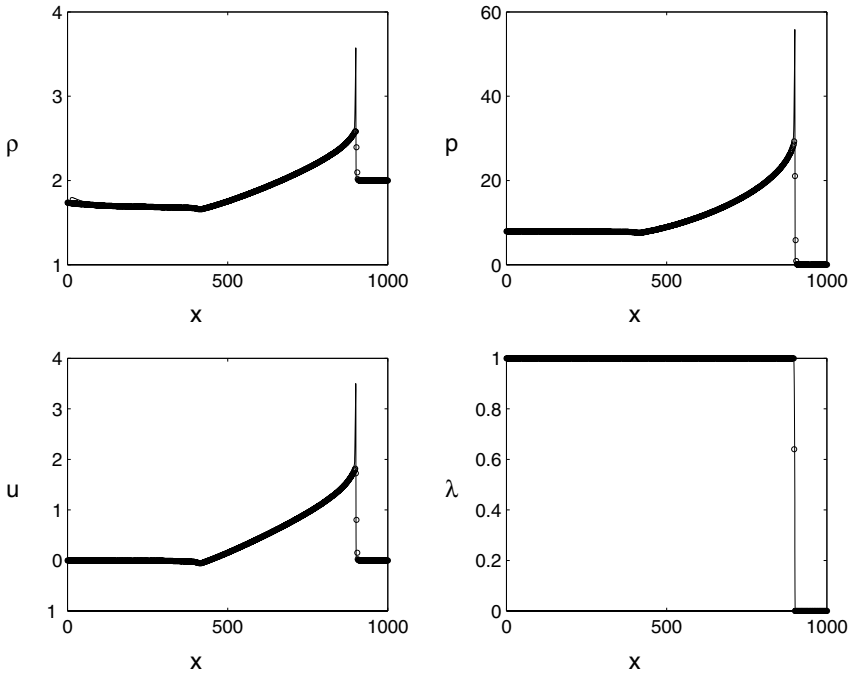

FIG. 29. Plot of the structure for cylindrical geometry with $\triangle x = 2mm$ at $x_s(t) = 900mm$. Circles correspond to the model TPB-3b ($t = 116.2\mu s$), and the solid curve to DNS ($t = 127.5\mu s$).

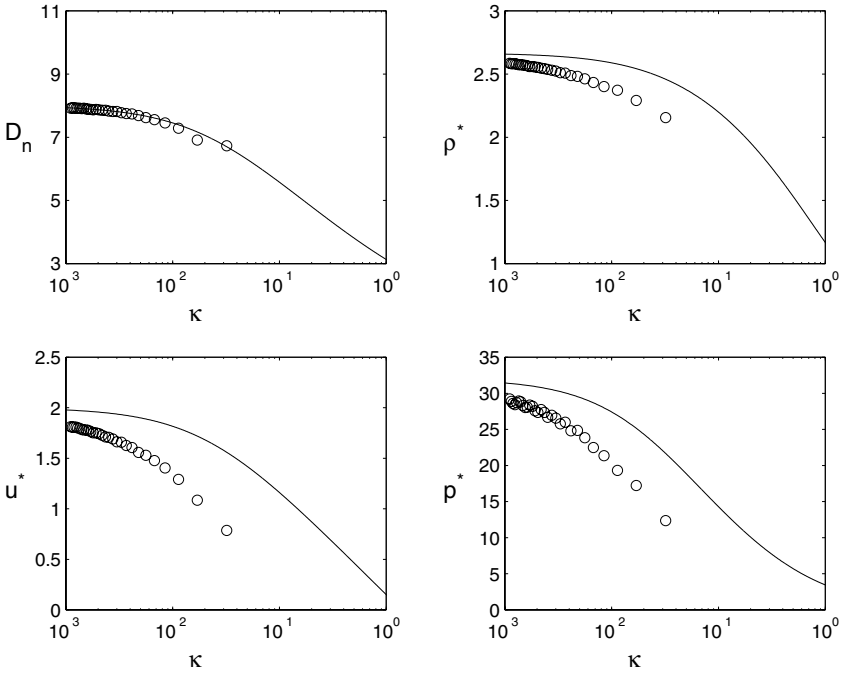

FIG. 30. Plot of D_n and the star states as a function of κ for DSD (solid) and model TPB-3b (circles) with $\triangle x = 2mm$.

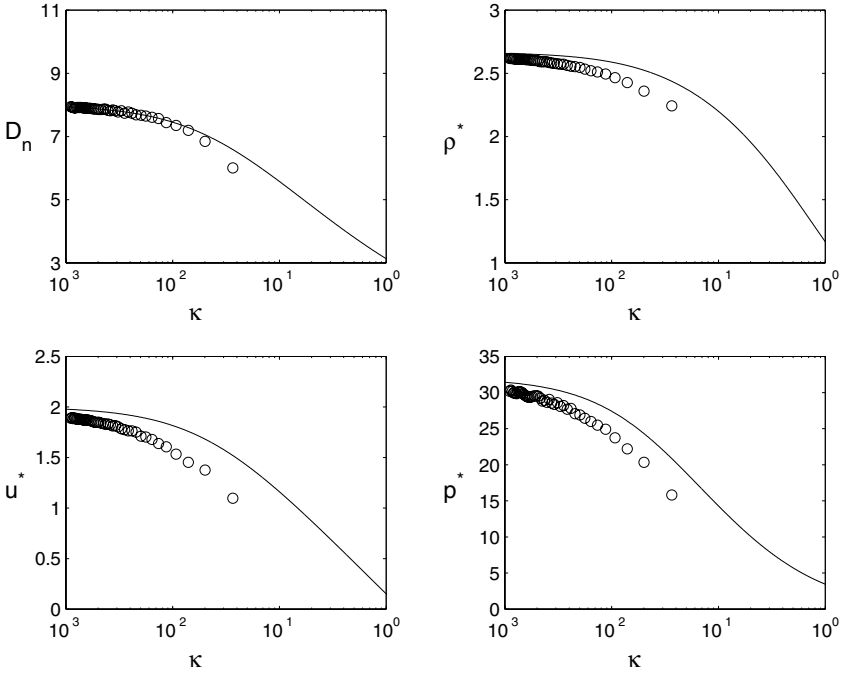

FIG. 31. Plot of D_n and the star states as a function of κ for DSD (solid) and model TPB-3b (circles) with $\triangle x = 0.5mm$.

REFERENCES

1. Aslam, T.D., Bdzil, J.B. and Stewart, D.S. (1996) "Level set methods applied to modeling detonation shock dynamics", J. Comput. Phys., 126, pp. 390-409.
2. Aslam, T.D. and Stewart, D.S. (1999) "Detonation shock dynamics and comparisons with direct numerical simulation", Combust. Theory Modeling, 3, pp. 77-101.
3. Aslam, T. D., Bdzil, J. B. and Hill, L. "Extensions to DSD-theory: Analysis of PBX9502 rate stick data", to appear in the *Proceedings of the Eleventh (International) Symposium on Combustion*, August (1998). Los Alamos National Laboratory Technical Release No. LA-UR-98-3884.
4. Bdzil, J. B, Aslam, T. D. and Stewart, D. S. (1997) "Resolved 3D Detonation Reaction Zones: Memory and Time Requirements for DNS", Los Alamos Report, LA-UR-97-792, Los Alamos National Laboratory, Los Alamos, NM.
5. Jiang, G.S. and Shu, C. (1996) "Efficient implementation of weighted ENO schemes", J. Comput. Phys. 126, 202-28
6. Shu, C. and Osher, S. (1988) "Efficient implementation of essentially non-oscillatory shock-capturing schemes", J. Comput. Phys., 77, pp. 439-471.
7. Stewart, D. S. (1998) "The Dynamics of Multi-dimensional Detonation in Gaseous and Condensed Phases Explosives: Topical Review", in the Proceedings of the 27th (International) Conference on Combustion, The Combustion Institute, pp. 2189-2205.
8. Whitham, G. B. **Linear and Nonlinear Waves** (1974) Wiley-Interscience pub., p. 277.
9. Wilkins, M. L. (1964) "Calculation of Elastic-Plastic Flow", in *Methods in Computational Physics*, *Advances in Research and Applications*, Volume 3, Fundamental Methods in Hydrodynamics, Alder, B., Fernbach, S. and Rotenberg, M. eds. Academic Press, pp. 211-262.
10. Xu, S., Aslam, T.D. and Stewart, D.S. (1997) "High resolution numerical simulation of ideal and non-ideal compressible reacting flows with embedded boundaries", Combust. Theory Modeling, pp. 113-142.